CHARACTERIZATION OF MOBILE PHASE FLOW INHOMOGENEITY IN MICRO-STRUCTURED FIBRES: TOWARDS THE DEVELOPMENT OF MULTI-CHANNEL SUPPORTS FOR OPEN TUBULAR LIQUID CHROMATOGRAPHY

by

JUSTIN WADE SMITH

A thesis submitted to the Department of Chemistry

in conformity with the requirements for

the degree of Master of Science

Queen's University

Kingston, Ontario, Canada

August, 2012

Abstract

Despite the prominent role played by open tubular columns in gas chromatography, they have enjoyed comparatively little success as supports for open tubular liquid chromatography (OTLC), owing to impractical channel diameters (3-5 µm) required to facilitate retention in the liquid phase. In an effort to circumvent the technical issues associated with such narrow diameters, columns with multiple parallel channels have been suggested as alternatives – to this end, micro-structured fibres (MSFs) have been proposed as supports for OTLC. Much research has been conducted using MSFs for chromatography in the Oleschuk group, and although some success has been achieved, performance has been continuously hindered by flow velocity variation among the channels stemming from differences in channel sizes (or channel variance) as well as differences in stationary phase coverage, which serve to degrade column efficiency. Recent efforts have focused on devising a novel method for assessing the channel variance of MSFs. This method seeks to determine hole tolerance through evaluation of the extent of band broadening that occurs when performing chromatography in the absence of a retentive mechanism. Using this method, a linear correlation between the relative standard deviation of the channel diameters and the amount of broadening was revealed. To supplement the results, computational fluid dynamics was employed to simulate fluid flow through multi-channel columns. The results of these simulations again provided a linear correlation between the RSD of the channel diameters and the extent of flow velocity variation among the channels.

Acknowledgements

First and foremost, I would like to thank my supervisor, Dr. Richard Oleschuk, for giving me the opportunity to study in his research group and guiding me throughout my graduate studies over the past two years. I also wish to thank the members of the "O" group for their support and friendship during my time in Kingston. I would especially like to thank Dr. Graham Gibson and Dr. Adam Daley for their guidance in the laboratory as well as Katerine Cossette for her guidance regarding computational fluid dynamics. I would also like to thank Dr. Natalie Cann and Dr. Igor Kozin for their willingness to serve on my supervisory committee.

I would further like to extend my gratitude to the Natural Sciences and Engineering Research Council of Canada and Queen's University for financial support I received throughout my studies.

Finally, to my family, I would like to thank you for your unwavering support during this time. It was difficult to be away from home for so long, but your love and reassurance over the years have allowed me to achieve my goals.

Table of Contents

List of Tables

List of Figures

List of Abbreviations

AU – arbitrary unit

C_{18} – octadecylsilane

CFD – computational fluid dynamics

CTMS – chlorotrimethylsilane

CV – channel variance

ESI – electrospray ionization

GC – gas chromatography

HCl – hydrochloric acid

HILIC – hydrophilic interaction chromatography

HPLC – high-performance liquid chromatography

i.d. – inner diameter

ID30 – inner diameter 30 µm

LC – liquid chromatography

MS – mass spectrometry

MSF – micro-structured fibre

m/z – mass-to-charge ratio

NaOH – sodium hydroxide

NP – normal phase

OTC – open tubular column

OTLC – open tubular liquid chromatography

PAH – polycyclic aromatic hydrocarbon

PDMS – polydimethylsiloxane

PLOT – porous layer-open tubular

PPM – porous polymer monolith

R_e – Reynold's number

RP – reverse phase

RSD – relative standard deviation

SEM – scanning electron microscopy

UDF – user-defined function

UPLC – ultra-high pressure-liquid chromatography (or ultra pressure-liquid chromatography)

Chapter 1: Introduction

1.1 Introduction to Chromatography

1.1.1 Fundamentals of Chromatography

Naturally occurring elements and compounds rarely exist in a pure state. Rather, they are generally found embedded within a complex matrix of impurities, and as such, a means of separation is necessary in order to purify the sample. Over time, separation science has evolved to afford a range of different techniques to fulfill this purpose, such as distillation, recrystallization, and liquid-liquid extraction. However, perhaps the most prominent separation technique in modern research is chromatography. Rapid development over the past several decades has forged chromatography into an extremely versatile and sensitive separation method, and it has since become an essential tool in nearly every facet of analytical science.

Chromatography is classified as a physical separation method that relies on a solute's distribution between two immiscible phases.[1] One phase is a porous bed immobilized onto a solid support (the stationary phase) while the other phase flows through it (the mobile phase). A sample mixture is dissolved in the mobile phase and allowed to travel through the support containing the stationary phase. A given solute, S, will distribute itself between the two phases based on its chemical interaction with the two phases, establishing the following dynamic equilibrium:[2]

$$S_{mobile} \rightleftharpoons S_{stationary} \quad (1)$$

Solutes migrate through the support only when they are in the mobile phase.[2] Therefore, solutes with a strong affinity for the stationary phase will migrate through the medium at a slower rate. Since each solute uniquely interacts between the two phases, they will experience different migration rates and, consequently, separation among the components will occur.

Contemporary chromatographic techniques such as gas chromatography (GC) and high-performance liquid chromatography (HPLC, also known as also known as high-pressure liquid chromatography) are exclusively carried out using cylindrical columns as supports.[3] With these techniques, a detector sensitive to solute concentration (or, in some cases, refractive index) is positioned at the end of the column as a means of observing analytes as they elute. Plotting the detector response as a function of time yields a series of Gaussian-shaped signals that represent the individual components of the mixture – such a plot is called a chromatogram. The time required for a solute reach the detector from its point of injection is called its retention time, t_r. A solute's retention time functions as a means of identifying the species. Furthermore, the signal can be used as a means of quantification as the area under the signal is proportional to the solute's concentration.[3] A commonly used expression used to describe a solute's retention is the retention factor, k (also known as the capacity factor), formally defined as the ratio of time an analyte is retained in the stationary phase to the time it is retained in the mobile phase.[1] It is given by:

$$k = \frac{t_r - t_m}{t_m} \quad (2)$$

where t_m is the mobile phase retention time (amount of time a solute takes to reach the detector in the absence of retention). An ideal range for k is between 1 and 5. Values below 1 generally result in irreproducible data because of excessively fast elution, whereas a value above 5 results in the solute being retained in the column for too long, leading to excessive band broadening.[2]

The Gaussian shape assumed by the signals is accounted for by a solute's natural tendency to diffuse longitudinally, forming discrete zones (or bands) as it migrates through the support.[2] A number of factors contribute to band broadening (see 1.1.2 Chromatographic Theory). Excessively broad signals can result in overlapping peaks, translating to poor resolution and separation performance, and as such, band broadening is largely undesirable. Although it cannot be eliminated, efforts can be made to minimize the extent of broadening through proper selection of the two phases along with optimization of the chromatographic parameters.

1.1.2 Chromatographic Theory

A quantitative description of chromatographic performance arises from a theory proposed by Martin and Synge,[4] in which a column is measured terms of theoretical plates. A theoretical plate (or simply, plate) is defined as a hypothetical zone within the column where a solute establishes equilibrium between the mobile phase and the stationary phase. According to the theory, solutes will spread along the length of a plate, and as such, columns that are divided into a greater number of plates effectively limit the extent of band broadening. Thus, the number of plates is proportional to the separation efficiency of the column.[4]

Two approaches to measuring theoretical plates exist: direct calculation the plate count (N), and measurement of the height equivalent of a theoretical plate (or simply, plate height, H). While individual columns are often expressed in terms of N, it prevents one from comparing the efficiency of columns that differ in length, since N is dependent on column length. It is therefore advantageous to measure H in order to make such a comparison. It is determined as follows:

$$H = \frac{\sigma^2}{L} = \frac{w^2}{16L} \quad (3)$$

where σ^2 is the signal variance, w is the base width of the peak ($w = 4\sigma$) and L is the length of the column.[2] From this, N is calculated by:

$$N = \frac{L}{H} = \frac{16L^2}{w^2} = \frac{16t_r^2}{w^2} \quad (4)$$

Since N is a dimensionless unit, L with t_r can be used interchangeably in determining the plate count.[2] The average plate height is dependent on the type of chromatography used: typical plate heights for the two most common chromatographic techniques, GC and HPLC, are approximately 0.5 mm and 10 µm, respectively.[2] Although these values seem to favour chromatography in the liquid phase, GC generally employs much longer columns due to lower viscosities that accompany the gas phase, affording comparable total plate counts to those encountered in HPLC.

A number of physical, kinetic, and thermodynamic variables dictate the overall plate height of a given column. Several theories and associated equations have been

proposed that attempt to quantify plate height from these contributions, such as those proposed by Knox,[5] Horvath and Lin,[6] and Giddings,[7] among others. However, the most commonly applied theory stems from the work of van Deemter and co-workers, who proposed the well-known van Deemter equation:[8]

$$H = A + \frac{B}{u} + (C_m + C_s)u \quad (5)$$

Each constant represents a different property of the column that contributes to band broadening:

- The A term represents the multi-path flow experienced by a solute migrating through a porous stationary phase bed, in which some pathways are shorter/longer than others. This term is also referred to as eddy diffusion.
- The B term signifies longitudinal diffusion due to the entropic tendency of a solute to migrate from concentrated center of the band to more dilute regions of lower concentration on each side. The value for B is dependent on the diffusion coefficient of the solute.
- The C terms each represent the rate of mass transfer for a given solute between the stationary phase (C_s) and the mobile phase (C_m). Lower values for C indicate that solutes require less time to equilibrate between the two phases. By contrast, larger values signify a resistance to mass transfer, causing solute molecules in the stationary phase to lag behind those in the mobile phase.

The term u represents the linear flow rate. It can be observed from the van Deemter equation that adjusting the flow rate has opposing effects on the B and C terms – increasing the flow rate lessens the amount of time that a solute spends in the column, which reduces the degree of longitudinal diffusion experienced, but also gives the solute less time to equilibrate between phases, thus increasing resistance to mass transfer. Decreasing the flow rate reverses the effect. Plotting the plate height as a function of flow rate reveals a hyperbolic function with a minimum value for plate height (H_{min}). The flow rate that corresponds with H_{min}, u_{min}, can be determined by the following calculation:[3]

$$u_{min} = \sqrt{\frac{B}{C}} \quad (6)$$

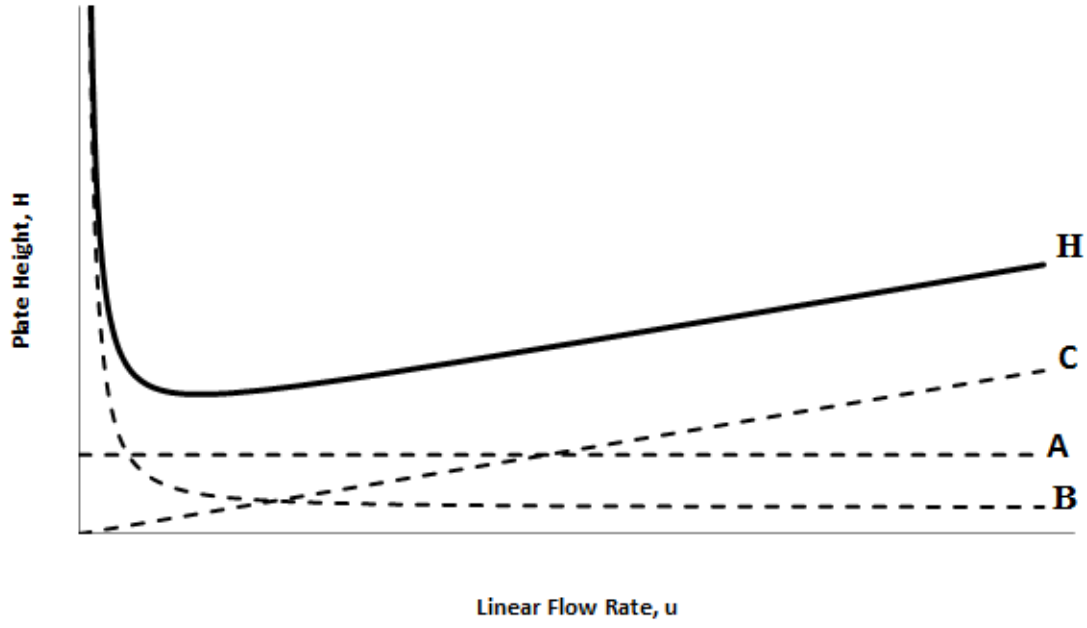

Figure 1.1: A generalized van Deemter plot.

1.2 High Performance Liquid Chromatography

1.2.1 System Components for HPLC

Modern advancements in separation science have afforded a wide range of chromatographic methods. Among them, perhaps the most widely used in current research is HPLC. Its acclaim stems from numerous factors, including its unprecedented versatility, high sensitivity and efficiency, ease of quantification, and automation.[9] As a tool in analytical research, HPLC is applicable in a number of fields, including environmental,[10,11] pharmaceutical,[12-14] and bio-analytical analysis.[15,16] Moreover, HPLC boasts the dual capability of performing both analytical and preparative separations, expanding its usefulness beyond chemical laboratories and into a number of industrial applications.[17,18]

HPLC employs pressurized flow supplied by a specialized pumping system to force a liquid mobile phase through the stationary phase. Conventional HPLC pumps are capable of generating highly reproducible mobile phase flow at pressures of up to 6000 psi (41,250 kPa), with volumetric flow rates of 0.1-10 mL/min.[2] The pump is connected to a number of solvent reservoirs from which the mobile phase is drawn. The use of multiple reservoirs allow for combinations of two or more solvents as the mobile phase – this is often preferred over using a single solvent as it provides a greater degree of control over the mobile phase's elution strength simply by adjusting the ratio between the solvents. Additionally, using multiple solvents allows the mobile phase composition to be varied during an analysis – a procedure known as gradient elution (as opposed to

isocratic elution, in which the mobile phase composition is held constant). Gradient elution allows one to continuously increase the elution strength (a measure of the mobile phase's interaction strength with the solute) during an analysis, leading to faster separation times without sacrificing resolution.[2] Ultimately, the choice of mobile phase depends primarily on the mode of separation to be used (see 1.2.3 Modes of Operation for HPLC).

The stationary phase is housed in a narrow, cylindrical column composed of stainless steel to prevent corrosion from contact with organic solvents.[3] The diameter of the column is dependent on the nature of the separation: larger bores (greater than 10 mm) are used in preparative HPLC, whereas smaller bores (1-5 mm) are used for analytical separations.[19] The bore diameter used in the majority of HPLC separations is 4.2 mm.[3] The sample injector is positioned in front of the column. Prior to each sample injection, the column is equilibrated with the appropriate mobile phase to ensure reproducibility among each separation. Additionally, a replaceable guard column is installed at the head of the main column. Its purpose is to mitigate damage to the column by removing particulate matter and other contaminants that could potentially bind irreversibly to the stationary phase.[3]

The detector is placed at the end of the column to record the retention time of eluting species. There is no universal detector that can be used in conjunction with HPLC – rather, an appropriate detector must be selected depending on the nature of the separation and the mixture in question. Absorbance detection is the most prominent

choice since most analytes absorb ultraviolet/visible light and its sensitivity is sufficient for the majority of applications. Detectors such as fluorescence and electrochemical detectors offer significantly lower detection limits than absorbance, but are limited in the number of compounds that they can detect.[20] Mass spectrometry (MS) has become an increasingly popular detection method due to the emergence of electrospray ionization (ESI), which enables it to be couple with HPLC (collectively known as LC-MS).[21] In addition to being highly sensitive, LC-MS provides the added advantage of being able to identify compounds based on its mass-to-charge ratio (m/z). However, it is a destructive technique, and so it cannot be applied in preparative HPLC without flow splitting.

1.2.2 Separation Media

Historically, the most commonly employed method for preparing HPLC stationary phases is through the use of spherical, micro-porous silica particles.[22] HPLC columns are packed with these particles, which serve as supports to which the stationary phase is bound. The surface properties of silica allows for easy functionalization through covalent bonding, resulting in highly robust materials that are resistant to dissolution in the mobile phase. Furthermore, the silica particles can be functionalized with a variety of different species, allowing one to choose an appropriate stationary phase for the desired mode of separation. The average diameter used in conventional packed columns is approximately 3-10 μm.[23] The micro-scale diameters afford a large surface-to-volume ratio, allowing for rapid mass transfer between the mobile phase and stationary phase,

which accounts for HPLC's exceptional sensitivity (this also rationalizes the high pressures needed to force the mobile phase through the support).

The particle size plays an important role in determining the plate height of a given column. Decreasing the particle diameter serves to elevate the surface-to-volume ratio, which increases the rate of mass transfer and consequently decreases the C term in the van Deemter equation.[23] Additionally, smaller particles allow for more uniform packing of the column, which reduces velocity bias and lessens the van Deemter A term. Unfortunately, smaller particles also increase the degree of flow-induced backpressure experienced; thus, a lower limit is imposed on diameter of particles that can be employed. This limit is dictated by the upper pressure restriction of the HPLC pump. Recently, Waters™ introduced ultra-high performance liquid chromatography (UPLC), which features pumps with pressure thresholds of up to 10,000 psi (68,750 kPa) – much higher than the 6,000 psi ceiling of conventional HPLC instruments.[24,25] This has enabled researchers to implement particle diameters below 2 µm, and corresponding decreases in plate height have been noted.[26] However, there is no direct way to increase the permeability of packed columns, and so operational limitations of available instrumentation will always be the defining factor for performance in this respect.

In an effort to circumvent the low permeability that limits packed column performance, porous polymer monoliths (PPMs) have recently garnered significant interest as a novel stationary phase for HPLC. PPMs are prepared using a combination of functional and cross-linking monomers in the presence of a porogenic solvent.[27] A

free-radical initiator (thermal or photolytic) is also added to initiate the reaction. The reaction initially produces numerous individual granules of polymer, which serve as the PPM backbone.[28] As the reaction continues, the granules swell and eventually reach a point where they become linked by further polymerization, generating a highly interwoven matrix among the backbone. As a separation medium for HPLC, PPMs offer porosities that are superior to traditional packed columns, allowing for improved mass transfer and, consequently, lower plate heights.[29] Furthermore, PPMs have the additional advantage of having a facile preparation procedure, requiring a single step to complete.[29] This procedure can be easily controlled simply by adjusting the amount of monomers, porogen, and initiator used, as well as through controlling the time of reaction. The high degree of control in PPM preparation additionally provides a great deal of versatility, allowing for a variety of different functionalities to be introduced into the framework.[30]

1.2.3 Modes of Operation for HPLC

Chromatography can be divided into several different modes of operation, based on the retention mechanism employed between the solute and the stationary phase.[2] The most commonly used separation mode for HPLC is sorption chromatography, whereby absorption and adsorption interactions between the solute and the stationary phase surface determines the retention time. Sorption chromatography for HPLC can be divided into two major sub-types: normal-phase (NP) and reverse-phase (RP) chromatography. NP-HPLC uses a polar stationary phase in conjunction with a non-polar mobile phase, whereas RP-HPLC reverses the two, using a non-polar stationary phase and a hydrophilic mobile phase.[2] The main difference between the two lies in the

type of compounds each technique can effectively separate: NP-HPLC is designed to separate non-polar compounds while RP-HPLC is used for separation of more polar compounds. Although this reciprocity seemingly establishes a complimentary affiliation between the two modes, NP-HPLC has fallen out of favour due to its susceptibility to drifting retention times – a result of the technique's high sensitivity to trace amounts of water in the mobile phase.[3] RP-HPLC, by contrast, is typically composed primarily of aqueous solvent, and is therefore much more robust to slightly fluctuating concentrations of water. Furthermore, the range of compounds separable by RP-HPLC can be extended by adjusting the mobile phase, either by using a more hydrophobic solvent or by including additives that assist in dissolving the mixture.

Partition chromatography, another separation mode, makes use of a retained liquid as the stationary phase, allowing solutes to partition between it and the mobile phase as a means of retention.[2] Historically, this approach has received little attention in HPLC, due in large part to the tendency of the liquid stationary phase to "bleed" from the column,[3] along with the widespread prevalence of RP-HPLC. However, it has experienced renewed interest in recent years as a result of the emergence of hydrophilic interaction chromatography (HILIC), a technique introduced by Alpert in 1990 that employs a very polar stationary phase (for example, silica) in conjunction with a hydro-organic mobile phase.[31] The organic component is generally either methanol or acetonitrile. Although the actual retention mechanism is an ongoing subject of debate,[32] it is generally theorized that HILIC operates via a unique partition mechanism whereby the aqueous component of the mobile phase, drawn by the hydrophilic stationary phase,

generates an aqueous layer along the stationary phase that is distinct from the bulk organic phase.[33] Its attraction to the stationary phase causes the aqueous layer to become partially immobilized and, consequently, it flows through the column at a slower rate than the bulk organic phase. The solute, which can partition between the two layers, undergoes retention as a result of this difference in flow velocities. HILIC's retention mechanism has been a subject of intense research due to its ability to effectively separate small, polar compounds, giving it strong applications in pharmaceutical and food research.[34] The range of compounds effectively separated via HILIC strongly overlaps with those that are suitable for NP-HPLC, making HILIC a viable alternative.[35] Moreover, HILIC's inherent reliance on an aqueous component obviates the need to keep the mobile phase dry, giving it a further advantage over NP-HPLC.

In addition to adsorption and partition, a wide range of other chromatographic modes exist, such as ion-exchange, size exclusion, and affinity chromatography.[2] These techniques, while extremely useful in numerous applications, are not as widely applicable as the modes discussed above. Since these modes fall outside the scope of this report, they will not be addressed.

1.3 Miniaturization of HPLC

1.3.1 Micro-column LC

Over time, analytical research has been continuously trending towards miniaturized instrumentation and technology. This movement has been prompted not only by the desire to reduce costs associated with research and laboratory usage and maintenance, but also by the myriad advantages that arise from the manipulation and analysis of increasingly minute sample volumes. The most obvious benefit of miniaturization is that it greatly reduces the quantity of sample required per analysis, which facilitates the use of rare and expensive compounds.[36] This is of further benefit to chromatographic techniques, which consume copious amounts of organic solvents during operation – in addition to lowering cost, the volume of solvent wasted is drastically reduced, which would otherwise pose an environmental threat.[37]

In accordance with the growing movement towards miniaturization, extensive effort has been devoted to scaling down HPLC separations. The development of miniaturized HPLC is closely tied to the pursuit of increasingly smaller particles for use as stationary phase packing material in an effort to improve separation efficiency.[25] Decreasing the size of packing particles, however, is accompanied by a significant increase in required operating pressure, resulting in a large accumulation of frictional heat in the mobile phase.[25] This generates a temperature gradient, which leads to excessive band broadening that is detrimental to column performance. While temperature gradients can be circumvented simply by reducing the column length, the

use of shorter columns does not improve separation efficiency, since the plate count is directly proportional to column length (although this approach does result in faster separation times).[38] A more effective approach to compensate for heat buildup is to use stationary phase supports with narrow channel diameters. Such columns offer more efficient radial heat dissipation, which prevents the generation of a temperature gradient when subjected to large pressure drops, and thus permits the use of smaller packing materials.[25] To this end, narrow-bore fused silica capillaries have been explored as alternatives to conventional stainless steel supports. This technique was first explored in the 1970s by various research groups,[39-42] who utilized capillary diameters of 100-300 µm. Their results, which frequently reported plate counts exceeding 100,000, led to an explosion of interest in micro-column LC, and it remains an active field of research today, with particles diameters as low as 1 µm being used.[43,44]

In addition to the prevention of heat build-up, reducing the column diameter also plays a direct role in improving overall separation efficiency. This was first noted in 1988 by Karlsson and Novotny, who assessed the separation efficiency of column diameters ranging from 44 to 256 µm.[45] Their results revealed that as the column-to-particle diameter ratio (also known as the Knox-Parcher ratio) falls below 6, a significant decrease in plate height is observed. This result was later rationalized by Jorgenson and Kennedy,[46] who revealed a number of factors that contribute to the observed lower plate heights. Firstly, the reduced column diameter limits the number of possible flow paths along which a solute can travel. This translates to an overall increase in diffusion between flow paths, allowing a solute to better sample all possible routes,

which lowers band broadening due to multipath flow.[46] Secondly, columns with smaller diameters can be packed with higher efficiency, which reduces velocity bias. This is primarily the result of the aptly-named "wall effect," which is described as follows: With conventional column diameters, there is significantly more space near the channel wall, leading to a higher overall flow velocity than through the center. Due to the significant improvement in separation efficiency, HPLC with column diameters below 100 μm are often alternatively labelled as nano-LC.[47]

Micro-column LC additionally features unique detection enhancements for certain detectors, allowing for greater sensitivity over its conventional counterpart. This is largely the result of the effect of chromatographic dilution, which is calculated by the following equation:[48]

$$D = \frac{\epsilon \pi r^2 (1 + k)\sqrt{2\pi LH}}{V_{inj}} \quad (7)$$

It is observed from Equation 7 that chromatographic dilution, D, is proportional to column radius, r, and as such, decreases in r correspond to a reduction in the extent of dilution. This is beneficial for concentration-sensitive detectors. An additional advantage is apparent through the use of mass spectrometric (MS) detection in conjunction with an ESI source (ESI-MS). A 1994 study by Wilm and Mann showed that electrospray ionization efficiency is improved as flow rate is lowered, resulting in excellent sensitivity at low flow rates such as those encountered in micro-column LC and especially nano-LC.[49] Much like nano-LC, this technique is generally independently

referred to as nano-ESI, owing to its unprecedented performance over conventional ESI-MS.

1.3.2 Instrumentation for Micro-column LC

In addition to the column dimensions, instrumentation plays an important role in the overall performance of micro-column LC. The system components must be able to accommodate the chromatographic parameters that are demanded by a given column. This is especially the case for micro-column LC – the low flow rates, small sample volumes, and high operating pressures that accompany the application of miniaturized LC columns impose highly stringent requirements that cannot be effectively handled using conventional HPLC instrumentation.

As a mixture traverses through the various components of a chromatograph, the solute band is subject to a number of dispersive effects characteristic of the system, causing the band to spread and ultimately degrade chromatographic resolution. These dispersive effects, collectively known as extra-column band broadening, arise primarily from void volumes that occur throughout the instrument.[50] A generally accepted criterion is that extra-column band broadening may decrease resolution by an arbitrary maximum of 5%.[48] Given the comparatively large dimensions and sample volumes and conventional and preparative HPLC, extra-column band broadening does not significantly diminish separation efficiency.[51] However, as column technology shifts towards miniaturization, the resulting analyte bands become considerably more tapered, rendering them highly sensitive to minor perturbations. To keep extra-column band broadening below the 5% cut-off, micro-column LC requires void volumes in the low

nano-litre range,[48] compared to the micro-litre volumes that are generally acceptable for conventional HPLC. Thus, the application of micro-column LC necessitates the assembly of very precise system components in order to minimize extra-column dispersion. This is especially the case with respect to the injector, which consists of numerous connections and flow passages. Additionally, the detector size must be reduced to compensate as well – in the case of absorbance detectors, flow cell volumes must be lowered to only a few nano-litres. Other considerations include the various connectors and valves, which can introduce significant dispersion if there are imperfections present.[50] Finally, it is recommended to use tubing diameters below 50 µm or, if possible, directly connect the injector and detector to the column to further eliminate broadening.[48]

A fundamental aspect of micro-column LC is that decreasing the column diameter also reduces the loading capacity of the column. As such, the use of sample volumes in the low micro-litre (and more recently, the nano-litre range) is necessary to prevent overloading the column.[50] For injections in the micro-litre range, conventional injection systems such as sample-loop valves and direct injection can be applied with acceptable performance, and such devices are commercially available. However, as volumes delve into the low nano-litre range (less than 20 nL), such injectors become ineffective due to excessive extra-column band broadening. Furthermore, the injection process becomes increasingly sensitive to pressure fluctuations, which diminish reproducibility.[50] To counter this, nano-litre injections have traditionally been accomplished through the use of a split vent installed between the injector and column

to deliver a small fraction of the actual injector volume.[52] Alternatively, on-column focusing techniques have been explored.[53] These techniques feature a packed pre-column installed before the main column, which serves to re-focus (or "stack") the analyte band prior to separation and thus enables one to circumvent the use of low nano-litre injections.

As previously mentioned, the reductions in particle size and column diameter that constitute micro-column LC give rise to significantly higher operating pressures and, consequently, lower volumetric flow rates. These parameters cannot be effectively handled by conventional HPLC instrumentation, which is designed to apply mL/min flow rates with a pressure ceiling of 6000 psi (41,250 kPa). By contrast, micro-column LC makes use of µL/min or nL/min flow rates and often encounter pressures much higher than 6000 psi. Thus, solvent delivery systems must be re-purposed to accommodate the pressure increase. To this end, direct pumping through the use of reciprocating pumps and syringe pumps has been successful for flow rates as low as 50 µL/min, and both are offered commercially.[48] For flow rates in the low µL/min or nL/min range, direct pumping is inapplicable, owing to a number of factors such as time-consuming flow equilibrium as well as slow column pressurization.[48] Furthermore, such pumps cannot reproducibly apply gradient elution due to pressure fluctuations that arise from the constantly changing viscosity of the mobile phase. To circumvent these obstacles, the use of flow splitting has traditionally been used. A major advance is the advent of ultra-high performance liquid chromatography (UPLC), introduced by Waters™ Corp. in 1999. UPLC features direct pumping as low as 200 nL/min and a

pressure ceiling of 10,000 psi (68,750 kPa).[25] Presently, UPLC instrumentation is commercially available from various suppliers in addition to Waters™.

1.4 Open Tubular Liquid Chromatography

1.4.1 Fundamentals of Open Tubular Liquid Chromatography

Open tubular columns (OTCs) present an alternative approach to preparing stationary phases for chromatography. Unlike packed columns and PPMs, which occupy the majority of space in a column, OTCs are designed to restrict the stationary phase to a definitive layer (or "film") along the column wall. This can be accomplished using two general methods; either by coating the channel wall with a viscous liquid stationary phase or through the use of a covalently bound support to which a stationary phase can be applied.[2] Regardless of the method used, the end result is an unobstructed pathway through the center of the channel, which leads to two useful advantages in terms of chromatographic performance: First, the central pathway reduces flow resistance experienced throughout the column, allowing for lower operating pressures and faster separations. Second, the open structure provides a singular path for solutes to travel, which virtually eliminates band broadening due to multiple pathways (the van Deemter A term). Consequently, OTCs are theoretically expected to express superior separation efficiency in comparison with packed columns.

The separation efficiency of OTCs is quantified by the Golay equation, which is given below:[54]

$$H = \frac{B}{u} + (C_s + C_m)u \quad (8)$$

On the surface, the formula looks identical to the van Deemter equation with the exception of the A term, which is absent. However, expansion of the B and C terms reveals several unique factors that influence the overall efficiency of OTCs, including the stationary phase film thickness (d_f), channel diameter (d_c), and the diffusion coefficient of the solute in both the stationary phase (D_s) and mobile phase (D_m).[55]

$$B = 2D_m \quad (9)$$

$$C_s = \frac{2k}{3(1+k)^2}\frac{d_f^2}{D_s} \quad (10)$$

$$C_m = \frac{1+6k+11k^2}{96(1+k)^2}\frac{d_c^2}{D_m} \quad (11)$$

where k is the capacity factor. It should be noted that although OTCs theoretically possess higher separation efficiencies than packed columns, the reduced surface-to-volume ratio of this format greatly limits the loading capacity of such columns, and therefore, longer columns are necessary in order to achieve optimal performance.

OTCs have endured a great deal of success as supports for GC analysis, and its usage and applications are well documented throughout the literature. By contrast, instances of open tubular liquid chromatography (OTLC) are notably infrequent. This discrepancy arises chiefly from the comparatively low diffusion coefficients that are encountered in the liquid phase, which gives rise to large resistance to mass transfer that diminishes separation efficiency.[56] To compensate, extremely narrow column diameters

are necessary in order to provide a sufficiently large surface-to-volume ratio that facilitates optimal mass transfer. A theoretical study by Jorgenson and Guthrie determined that optimal column diameters for OTLC lie in the range of 1-3 μm (as a point of comparison, optimal OTC diameters for GC fall within a much more feasible range of 200-300 μm).[57] The use of such narrow columns is highly impractical as a result of the severe flow resistance that is encountered, which requires flow rates of just a few nL/min in order to perform.[56] Moreover, the loading capacity of such columns is extremely small, which not only requires sophisticated injection systems, but also necessitates a highly sensitive detector.[57] Hence, early attempts to perform OTLC were rare and generally met with poor results.[45]

In an effort to circumvent the heavy instrumental requirements that accompany OTLC, a number of techniques have been devised to enable more practical column diameters to be employed. One such method is the use of thick stationary phase films. Early attempts to perform OTLC centered on the preparation of thin wall-coated films as stationary phases; for example, C-18 monolayers.[58] Such techniques, while easy to implement, feature low surface areas which require the aforementioned 1-3 μm column diameters in order to facilitate an acceptable degree of retention. The use of thick films, by contrast, affords a much greater surface area and allows larger column diameters to be employed.[58] This enables more practical loading capacities and, consequently, less stringent instrumental requirements in terms of sample injection and detection. However, the increased loading capacity of thick-film OTLC comes at the expense of a reduction in chromatographic performance as a result of an increased resistance to mass

transfer in the stationary phase, which severely limits performance as film thickness increases.[54,59]

In addition to thick films, performing OTLC at elevated temperatures has been suggested as an avenue to using larger column diameters. This technique is predicated on the fact that raising the temperature leads to a more rapid rate of diffusion, thus as a result increasing the rate of mass transfer and allowing for larger diameters to be employed. It has be demonstrated that, using high temperature OTLC, column diameters of up to 50 µm can attain theoretical plate heights exceeding one million.[60] However, these advantages are offset by the need for additional instrumental components that are necessary to avoid vaporization of the mobile phase.[61] Furthermore, high temperature OTLC is limited to the analysis of thermally stable and non-volatile compounds, both of which are typically more suited to GC analysis.[58]

The technological advancements that have come from the pursuit of HPLC miniaturization has led to a revived interest in OTLC in recent years. Current HPLC instrumentation is capable of reproducible flow rates as low as 20 nL/min along with low nano-litre sample injections,[62] both of which lend to the feasibility of using sub-10 µm columns. Furthermore, the emergence of nano-ESI has provided nano-scale separations with a highly sensitive means of detection,[62] and is thus capable of measuring the miniscule sample volumes needed for OTLC. Having addressed the instrumental concerns, the remaining challenge is the preparation of a uniform stationary phase layer. To this end, polymeric stationary phases prepared in porous layer open

tubular (PLOT) format have expressed the greatest success in recent years. Polymeric stationary phases are advantageous in that they can be easily tailored to adopt a variety of chemical properties, making them highly versatile and able to accommodate numerous separation modes.[63] Furthermore, preparation of polymeric stationary phases typically features a one-step polymerization reaction, a procedure that is relatively facile in comparison to packing columns.[63] Moreover, the reaction conditions can be easily manipulated, allowing for a high degree of control over the thickness of the polymer layer.[54] The use of polymeric stationary phases for OTLC has been recently demonstrated in several articles by Karger and co-workers who, using a column diameter of 10 µm, prepared a polystyrene/divinylbenzene stationary phase for analysis of peptides.[62] Combined with nano-ESI detection, more than 1000 peptides spanning hundreds of different proteins were effectively separated and characterized. The effectiveness of this method has led various scientists to speculate the value of polymeric PLOT columns in proteomics.[64-66] The group followed up on this success with the preparation of an amine-bonded poly(vinylbenzene chloro-divinylbenzene) stationary phase for the separation and analysis of glycans in HILIC mode,[67] an example that further highlights the versatility of polymeric stationary phases.

1.4.2 Multi-channel Supports for Open Tubular Liquid Chromatography

In spite of the recent achievements in terms of LC instrumentation, detection, and stationary phase development, OTLC remains primarily a laboratory phenomenon. The highly specialized equipment required to perform OTLC, combined with the adversity in manufacturing columns with extremely narrow bores, makes the technique highly inaccessible, and as such, it is a largely neglected topic among the scientific community. In an effort to make OTLC more accessible, the use of supports with multiple parallel channels has been proposed.[68] Multi-channel supports are beneficial in that they increase the overall column volume, leading to greater loading capacities which ease the instrumental requirements for sample injection and detection. Furthermore, the division of mobile phase flow across multiple channels serves to alleviate flow resistance, allowing for operating pressures and flow rates that fall within more reasonable ranges. Overall, multi-channel supports enable the use of very narrow channel diameters without imposing stringent operating parameters.

Multi-channel columns were first demonstrated in 1976 by Janik and co-workers, who prepared a multi-channel GC column by filling a capillary with several solid rods and using the interstitial spaces between them as flow channels.[69] Although these columns were criticized for their non-uniform channel dimensions, the columns were successful in demonstrating the higher loading capacities possible with multi-channel supports. Later work by Pierce featured glass capillaries which were bundled together in a glass casing, then drawn in a similar manner as a conventional capillary.[70] This method featured cylindrical channels and smaller distribution of channel sizes, but

technical difficulties in preparing the columns resulted in severe non-uniformity among the channels, thus preventing the columns from performing acceptably.

In theory, multi-channel columns are capable of separations with efficiencies in excess of millions of plates.[68] However, this theory is predicated on the assumption that all of the channels are identical in terms of both size and shape. In reality, such a feat is near impossible to achieve, as witnessed in the work of Janik and Pierce.[69,70] Due to manufacturing imperfections and poor precision at the micro-scale, multi-channel columns inherently possess a distribution of channel diameters that are inconsistent not only among each other, but also along the length of the channel. The result of this distribution is a variation of mobile phase flow velocities among the channels. This observation is accounted for by the Hagen-Poiseuille equation, a formula encountered in fluid dynamics that describes the pressure drop of a fluid as it flows through a cylindrical channel, assuming incompressible, laminar flow:[71]

$$\Delta P = \frac{8\mu LQ}{\pi r^4} \quad (12)$$

where:

- ΔP = Pressure drop
- μ = Viscosity
- L = Channel length
- Q = Volumetric flow rate
- r = Channel radius

It can be seen from Equation 12 that a direct relationship exists between Q and r. Of particular importance is the fact that r is raised to the fourth power, signifying that even slight discrepancies in channel size will have a profound effect on the flow rate (assuming that the pressure drop remains constant). A study by Meyer predicted that in order for multi-channel supports to compete with packed columns in terms of plate heights, variation in inter-channel flow rates must not exceed 1%.[68] Thus far, this goal has yet to be achieved, and as such, multi-channel chromatography continues to express low plate efficiencies that fail to make it competitive with established methods.[72-74]

1.4.3 Micro-structured Fibres as Supports for Open Tubular Liquid Chromatography

A recent addition to the fibre optics industry, photonic crystal fibres (alternatively termed micro-structured fibres, or MSFs) are a class of optical fibre that features a periodic array of micro-channels. They are fabricated through the use of a macroscopic pre-form – an assembly of glass rods that assume the required array pattern. The rods are then fused together and drawn using a standard fibre drawing tower, much like a standard fibre would be drawn. This "stack-and-draw" procedure is highly versatile in that the hole pattern can be altered simply by making the appropriate adjustments to the pre-form.[75] The hole pattern is an important consideration in the manufacture of MSFs, as it impacts their optical properties.[76] As a result, a variety of MSF patterns exist, each with unique optical characteristics. The exceptional optical properties of MSFs, along with their versatility, have established them as an important tool in fibre optics with numerous applications.[75]

Although the original intention of MSFs was for use as light guides, their geometrical design suggests that they may be suitable for other applications, especially in analytical chemistry. To date, MSFs have been applied as supports for electrophoresis,[77] as gas phase sensors,[78] and as emitters for nano-ESI.[79] In addition to these, MSFs hold potential as novel multi-channel supports for chromatography. With an average channel diameter of 3-5 µm, MSFs possess diameters comparable to the theoretical requirements for OTLC, as outlined by Jorgenson and Guthrie. Moreover, the procedure used to manufacture MSFs produces low variance between channel diameters. Additionally, MSFs are typically composed of fused silica, providing them with functionality to which a stationary phase film can be anchored. Finally, the outer diameter of MSFs (~350 µm) are approximate to that of conventional capillary columns (~365 µm), allowing them to interface with current instrumentation. To date, only one publication exists outlining the use of MSFs as supports for OTLC.[80]

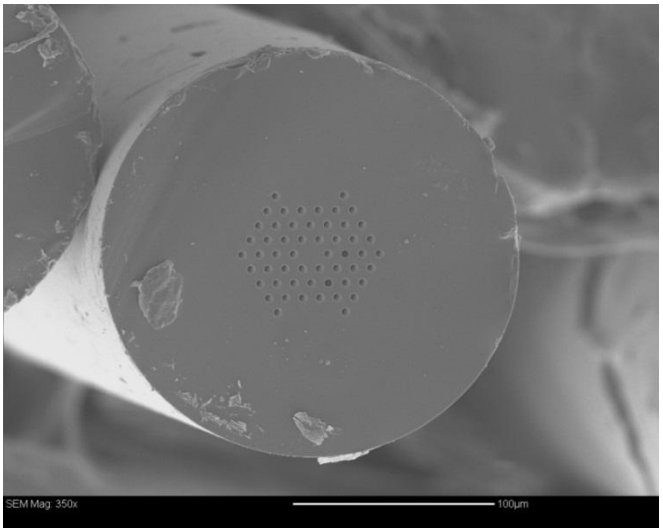

Figure 1.2: Scanning election micrograph of a micro-structured fibre cross-section.

1.5 Project Objectives

The central theme of my research is the development of MSFs as supports for OTLC. To this end, my project is divided into two sections – the first part focuses on the modification and evaluation of MSFs and their viability as open tubular chromatographic supports. An exploratory approach was investigated whereby the bare walls of the MSF channels assume the role of the stationary phase. It is hypothesized that since the MSF channels, being made of silica, are highly polar, they may be sufficient to serve as a polar stationary phase for HILIC, thus obviating the need to add a stationary phase to the column.

In addition to the assessment of MSFs for OTLC, a novel procedure for characterizing liquid flow through multi-channel supports is proposed. It is accomplished by injecting a standard solution containing a single analyte through a column and performing chromatographic analysis under conditions of no retention, resulting in a broad, singular peak (or "plug") to appear in the chromatogram. The difference in time between the beginning and end of the plug (the peak width) is dependent on the extent of flow variation among the channels, and as such, supports with a greater degree of variation between channel diameters are expected to generate wider plugs. This method provides a more accurate and comprehensive analysis of channel variation in MSFs than a cross-sectional SEM image, which has traditionally been used to assess channel variation. To supplement the flow characterization data acquired for MSFs, the experimental procedure was replicated using computational fluid

dynamics (CFD) software. The data from these simulations were then used as a point of comparison for the experimental data obtained from the characterization of flow through MSFs.

Chapter 2: Development of Micro-structured Fibres as Multi-channel Supports for Open Tubular Liquid Chromatography (Past and Current Research)

2.1 Introduction

2.1.1 Summary of Past Research

Development of MSFs for OTLC has been an ongoing endeavor in the Oleschuk laboratory for the past three years, with focus centred on effective preparation of open tubular stationary phases (or films) along the channel walls. During this time, various approaches to functionalizing the channel walls of MSFs with stationary phase films have been explored. Initial efforts were aimed towards preparing polymeric stationary phases using polystyrene/divinylbenzene in porous layer open tubular (PLOT) format; this direction was based upon the recent success of polymeric PLOT columns for single-channel OTLC, as demonstrated by Karger and co-workers.[62] To evaluate column performance, a binary mixture of polycyclic aromatic hydrocarbons (PAHs) was prepared and analyzed via reverse-phase chromatography. The resulting chromatogram, however, featured a multiplicity of signals for each sample component. This result signified that excessive variation of mobile phase flow velocities among the channels, which translated to a staggered emergence of analytes from the column channels (Figure 2.1). Although the differences in channel diameters inherent from the manufacturing of MSFs expectedly contribute to the observed flow variation, a more significant source in the case of PLOT columns originated from the introduction of the stationary phase. The unpredictable nature of the free-radical reaction governing stationary phase development

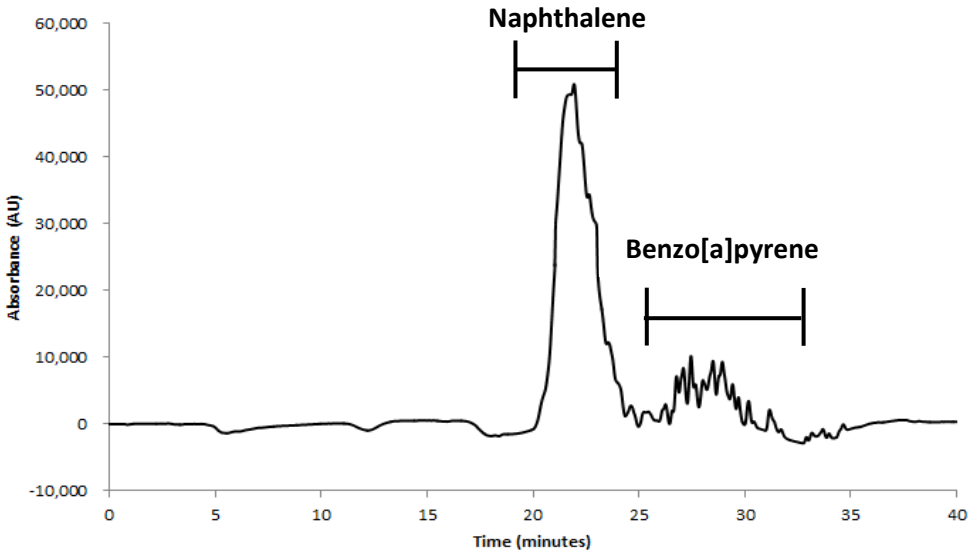

Figure 2.1: Early separation of a binary mixture of PAHs using an MSF functionalized with a polystyrene/divinylbenzene stationary phase. A gradient of 10-99% acetonitrile/deionized water over 15 min was used at a flow rate of 400 nL/min.[81]

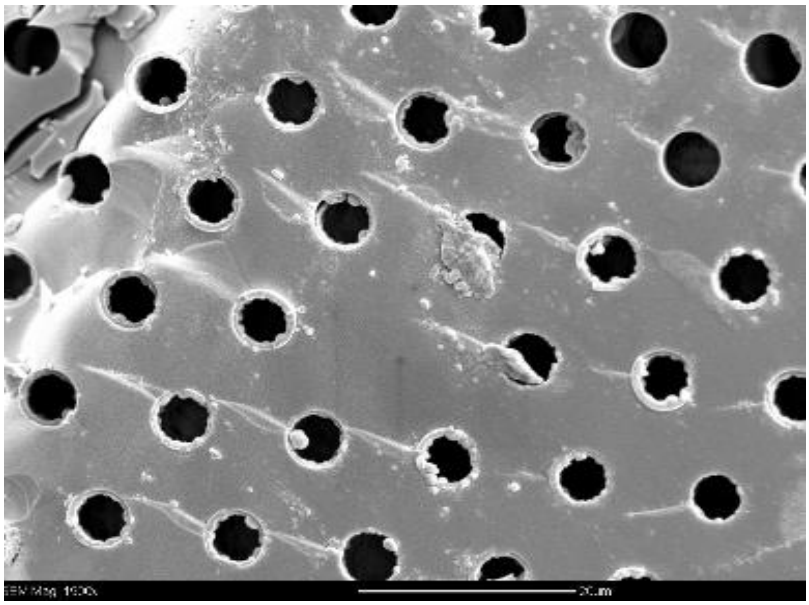

Figure 2.2: Scanning electron micrograph of a MSF functionalized with a polystyrene/divinylbenzene stationary phase.[81]

resulted in a diversity of film morphologies from channel to channel (Figure 2.2), which in turn generated severe heterogeneity among inter-channel flow velocities. Regardless of the selection of monomers and reaction conditions, the issue persisted, and it was eventually concluded that polymeric stationary phases were unsuitable for multi-channel OTLC.[81]

Given the incompatibility of polymeric PLOT films with multi-channel OTLC, a new direction was taken using octadecylsilane (C_{18}) monolayers as stationary phases for reverse-phase OTLC. The monolayers were prepared via a simple silanization reaction between the chlorosilane and the silanol groups that exist on the channel walls. It was expected that, since the reaction was limited to the channel walls, a more uniform film would result (relative to the films afforded by polymers). The implementation of monolayers for OTLC has been criticized in the past because of the poor surface area that they provide, which necessitates the use of 1-3 μm column diameters to achieve a sufficient surface area-to-volume ratio.[54,58] While the use of such narrow diameters stands as a significant obstacle for single-channel OTLC, multi-channel supports greatly increase the feasibility of implementing the necessary diameters for monolayers. Moreover, MSFs in particular possess average diameters that are slightly above this range, making them reasonable candidates for monolayer stationary phases. Using C_{18} columns, simple mixtures containing up to four PAHs could be effectively separated, and the results overall featured a significant improvement over analogous experiments using PLOT columns, with fewer and less pronounced peak multiplets appearing.[81] However, the poor resolution and continued persistence of peak multiplicity suggested

that heterogeneity among channel diameters was still an issue. An additional concern was that the silanization reaction likely did not reach completion, resulting in discrepancies in stationary phase coverage between channels, leaving behind unreacted silanol moieties that would disrupt the retention mechanism and, as a consequence, cause retention to differ among the channels. To counter this issue, trichlorosilanes were substituted with monochlorosilane analogues, which were expected to provide a higher degree of uniformity (as there is only one chlorine available to react, giving the silanes only one bonding configuration instead of three) (Figure 2.3).[81] Additionally, C_{18} functionalized fibres were treated with chlorotrimethylsilane (CTMS) to "cap" any unreacted silanols, preventing them from affecting separations.[81] Both alterations led to noticeable improvements in resolution, although performance was still not sufficient to compete with conventional HPLC techniques.

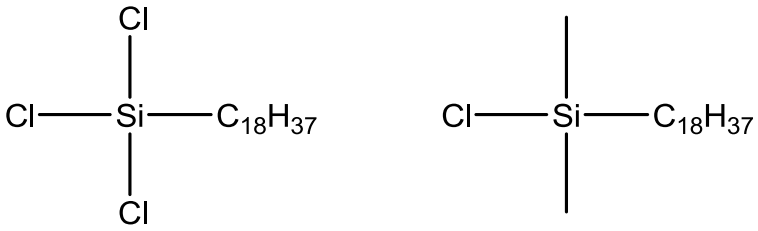

Figure 2.3: Molecular structure of trichlorooctadecylsilane (left) and chlorodimethyloctadecylsilane (right).

More recently, a third avenue to preparing MSFs for OTLC featuring the use of fluorous stationary phase films was investigated.[80] Fluorous chemistry (i.e. chemistry involving perfluorinated compounds) offers a unique means of separating compounds that takes advantage of unique fluorine-fluorine affinities, providing a strong, highly selective interaction mechanism that is less prone to non-specific retention.[80] The stationary phase was prepared as a monolayer using the same silanization reaction as the C_{18} monolayer, the only exception being that a perfluorinated C_{18} chlorosilane was used (Figure 2.4). Using this stationary phase, a mixture of fluorous-tagged triphenylphosphine oxides were separated with exceptional efficiency compared to previous efforts. Of particular interest was the near complete absence of peak multiplets for optimized experiments – a major improvement over the original C_{18} experiments. The results from these experiments are currently the only publication in the literature detailing the use of MSFs for OTLC.[80] It should be noted, however, that despite improved performance displayed by fluorous OTLC, the separation efficiency and resolution are still far from being competitive with conventional methods.

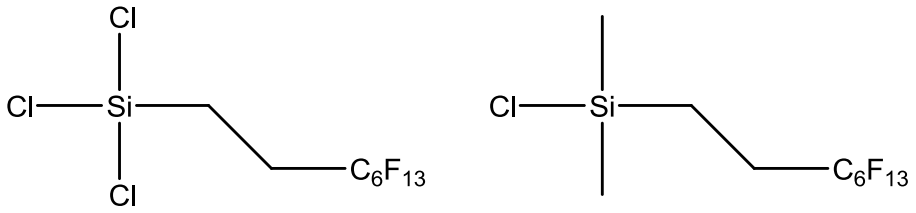

Figure 2.4: Molecular structure of trichloro(1H,1H,2H,2H-perfluoroctyl)silane (left) and chlorodimethyl(1H,1H,2H,2H-perfluoroctyl)silane (right).

2.1.2 Summary of Current Research

Although the progressive improvement in chromatographic performance of MSFs is promising, the studies previously discussed clearly illustrate that flow variation stemming not only from channel diameter heterogeneity but also from stationary phase discrepancies is an ongoing developmental barrier which must be rectified if progress is to continue. To address this, my research aims to develop an alternative approach to utilizing MSFs as supports for OTLC through the exploitation of the MSF channel walls, which are composed of silica, as stationary phases. The use of underivatized silica as a stationary phase for HILIC has been proposed previously in the literature.[82] Since silica (more specifically, the silanol groups inhabiting the silica surface) are highly polar, it was hypothesized that the MSF channel walls could serve as a stationary phase for HILIC. Using this technique, the need to introduce a stationary phase is obviated, thereby eliminating a major source of flow variation that has hindered the chromatographic performance of MSFs in the past.

In addition to introducing a new approach to using MSFs for OTLC, my research also seeks to address some procedural concerns regarding the preparation of MSFs as chromatographic supports. In the past, MSFs were directly installed onto the LC instrument after preparation of the stationary phase. However, this method has been problematic as contact with organic solvents from the mobile phase would cause the acrylate coating of the MSF to erode and detach from the fibre core. This issue required that the fibre ends be cut (approximately 1-3 cm) after each use to be able to reconnect the column. To address this problem, a procedure for modification of the fibre ends was

introduced. This procedure involved the use of polyimide-coated fused silica capillary columns, which were slid onto the bare fibre ends whose coating was previously removed. Since they are resistant to organic solvents, the capillaries are expected to improve the robustness of the MSF columns, enabling longer and more durable usage.

2.2 Experimental

2.2.1 Chemicals and Materials

All aqueous samples were prepared using deionized water purchased directly from Fischer Scientific (Middletown, VA, USA). Hydrochloric acid, sodium hydroxide, HPLC grade acetonitrile, and acetone were obtained from Fischer Scientific (Nepean, ON, Canada). Uracil was generously donated by the David Zechel group at Queen's University. AngströmBond® epoxy adhesive was purchased from The Fibre Optic Center (New Bedford, MA, USA). All chemicals were used as received.

Micro-structured fibres were purchased from NKT Photonics (Birkerød, Denmark). Only one variety, the 54-hole fibre (LMA-PM-15), was used. A cross-sectional image is given in Figure 2.5. It featured channels aligned in a uniform, hexagonal pattern in the center of the fibre (Figure 2.4). Polyimide-coated capillaries were obtained from Polymicro Inc. (Phoenix, AZ, USA).

2.2.2 Scanning Electron Microscopy

Scanning electron microscopy (SEM) images of the MSF was acquired using a Jeol JSM-840 scanning electron microscope (Tokyo, Japan). Several small pieces of the fibre (approximately 1 cm each) were cut and stripped of their acrylate coating by immersing them in acetone for approximately two minutes. The bare fibres were then mounted onto an aluminum stub using masking tape, with the fibre cross-section facing upward. The fibres were gold-coated using an Anatech Hummer 6.2 Sputtering System (Hayward, CA, USA) for three minutes prior to SEM imaging. Using the SEM images, the average diameter of the channels was measured and from this data, the volume of the MSF was determined.

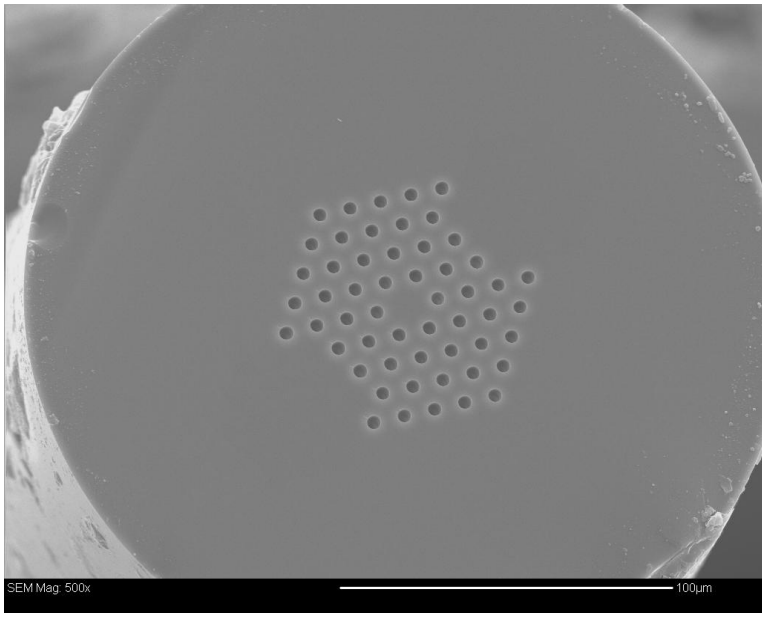

Figure 2.5: SEM of 54-hole MSF cross-section.

2.2.3 Preparation of MSFs

MSFs used for chromatography were cut to a length of 100 cm using a ceramic cutter. On each end of the fibre, 5-8 cm was immersed in acetone for approximately 2 minutes and then manually stripped away from the fibre. The unprotected core of the fibre, which had an inner diameter (i.d.) of approximately 240 µm, was then fitted with a polyimide capillary (i.d. 250 µm) of slightly shorter length such that about 1 cm the fibre extruded from the capillary. As the capillary was slid on, the bare fibre was dabbed with AngströmBond® epoxy adhesive using a wooden stir stick. The capillary was constantly rotated in both directions during the application of adhesive to promote better coverage throughout the circumference of the fibre. An illustration of the modification procedure is given in Figure 2.6. The fibre was then placed in an oven at 100°C for two hours to allow the epoxy to cure. Afterwards, the portion of bare fibre extruding from the capillary at each end was cut using a ceramic cutter to ensure that the channels were not blocked with epoxy. The column was then ready for chromatography.

After initial chromatographic testing, MSFs were subjected to a sequential etching treatment. This was performed by flushing the capillary with each of the following, in order: 0.1 M sodium hydroxide (NaOH), deionized water, 0.1 M hydrochloric acid (HCl), and finally deionized water. A Harvard Apparatus 11 plus syringe pump was used to flush the MSFs at a flow rate of 0.500 µL/min. NaOH and HCl were set to flush for approximately one hour each. Flushing with water was halted once the eluting solution was at an approximately neutral pH, as determined using pH paper (Micro Essential Laboratory, Brooklyn, NY).

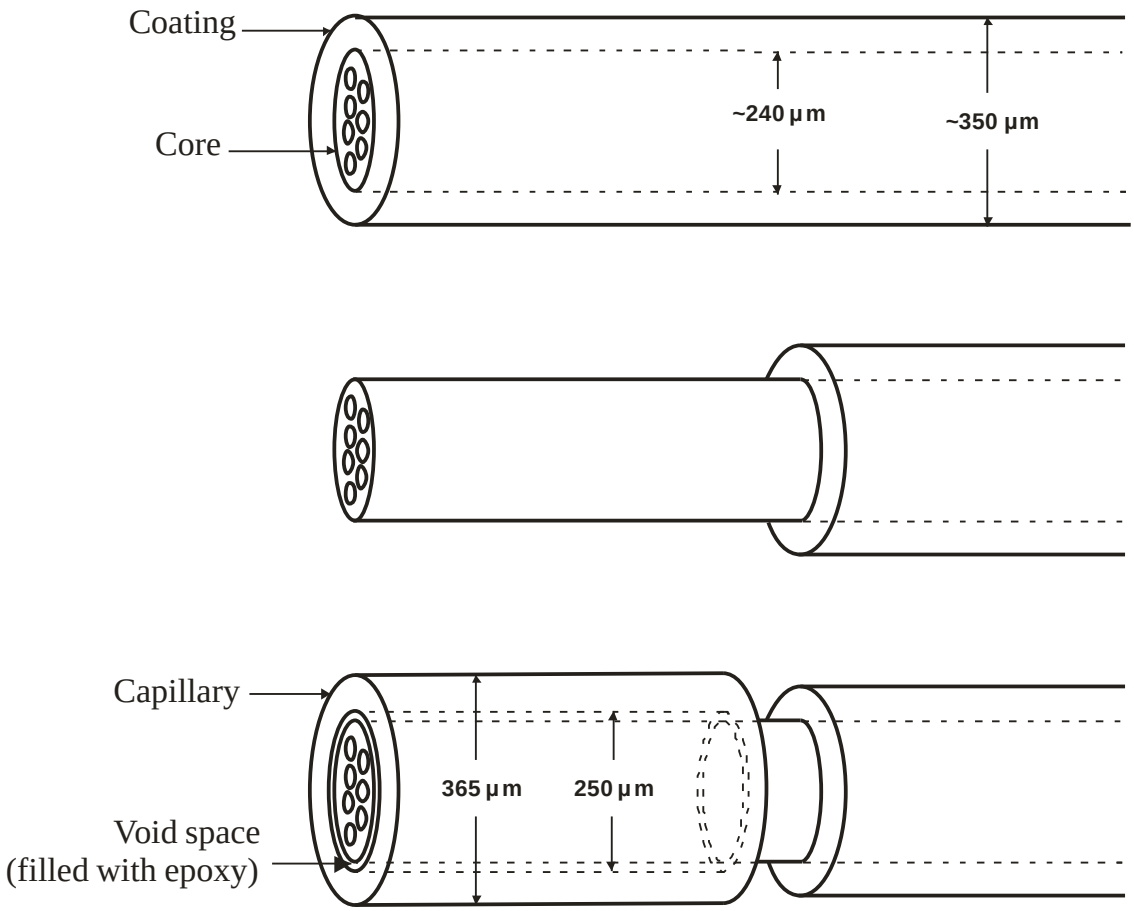

Figure 2.6: Procedure for modifying MSF ends with fused silica capillary.

2.2.4 Sample Preparation

Uracil was chosen as the test analyte. This choice was based on the recent success of HILIC in the separation of purine and pyrimidine bases.[83] A stock solution of 50-100 µg/mL was prepared in deionized water. All samples used for analysis were diluted to final concentrations of 5 µg/mL in 95% acetonitrile/5% deionized water.

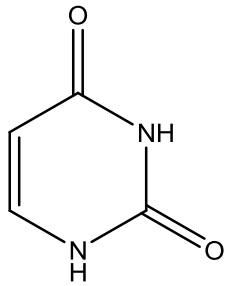

Figure 2.7: Molecular structure for uracil.

2.2.5 Chromatography

All chromatographic experiments were performed using a Waters nanoAcquity UPLC system fitted with a tunable ultraviolet absorbance detector (Milford, MA, USA). Instrumentation was operated using MassLynx (v 4.1) software. Columns were coupled to both the detector and the injector using NanoTight unions (P-779-01) and MicroTight Fittings (F-125X), both obtained from Upchurch Scientific (Oak Harbor, WA, USA). The detector wavelength was set to 260 nm for all experiments. No temperature control was implemented.

The injection valve was equipped with a 2 µL sample loop, and a full-loop injection was used to introduce samples. The use of such a relatively large loop volume is precarious in that it is significantly larger than the total volume capacity of the fibre

used – the total volume within a 54-hole MSF at 100 cm length is approximately 697 nL – which could potentially overload the column. However, the actual amount of analyte that is injected at any given time was calculated to be less than 50 ng, which is comparable to similar publications. Furthermore, it has been previously determined by the Oleschuk group that the injection volume has a relatively negligible effect on the extent of band broadening.[84]

For the analysis of uracil using HILIC, the mobile phase was 95% acetonitrile/5% deionized water. Separations were performed under isocratic elution conditions. The flow rate for all experiments was 400 nL/min.

2.3 Results and Discussion

2.3.1 Preparation of MSFs

Due to the extreme fragility of fused silica fibres at micron-sized diameters, MSFs are insulated in a polyacrylate-based coating to prevent them from breaking under stress. However, acrylates are sensitive to contact with organic solvents, which cause them to swell and eventually detach from the fibre (it should be stressed that MSFs were not originally designed for the purpose of chromatography). This makes using MSFs with HPLC a precarious task as the mobile phase routinely comes into contact with the coating at the fibre ends during chromatography, which compromises the connection between the column and the instrument. This is further exacerbated by the fact that the acrylate coating is relatively elastic, making it difficult for the fittings to clamp down tightly onto the fibre and keep it in place. A proposed solution to this issue was to

remove the coating at both ends of each fibre and replace it with an appropriate length of polyimide-coated fused silica capillary. This technique afforded numerous advantages in terms of column installation and durability. First, the polyimide coating of the capillary is resistant to contact with organic solvent. Thus, by fitting the fibre ends with capillary, the issue regarding swelling of the acrylate coating is circumvented. Additionally, capillaries afford a greater degree of durability over the acrylate coating, and thus the modified columns provide greater robustness. Modification of the fibre ends with capillary is further advantageous as it affords a better connection with the fittings used, since the outer diameter of the capillary is closer to the inner diameter of the sleeves used in the connections. By contrast, MSFs with the acrylate coating intact have slightly smaller outer diameters which make them susceptible to slipping out of the sleeve, especially upon prolonged contact with the mobile phase.

A complicating factor in the modification of MSFs with capillary is keeping the capillary fastened to the fibre. Since the outer diameter of the fibre core (approximately 240 μm) is slightly smaller than the inner diameter of the capillary (250 μm), there is significant void space throughout which the capillary can move. Thus, to keep the capillary fastened to the fibre, the void space was filled with an adhesive during placement of the capillary. The addition of an adhesive was useful not only to affix the capillary to the fibre, but also to prevent liquid from leaking through the void space between the capillary and fibre. Several materials were screened as potential candidates to keep the capillary in place. Originally, polydimethylsiloxane (PDMS) was used. However, it was found to be a poor adhesive which failed to bind strongly to the fibre or

capillary, causing the capillary to detach from the fibre after only a few chromatographic runs. Speed Set™ 5-minute epoxy was also attempted, but was very viscous, making it difficult to effectively apply to the fibre and in most cases the fibre broke during implementation of the capillary. Furthermore, those that did work featured similar results to PDMS. Eventually, AngströmBond® epoxy adhesive was explored as a candidate, and performed admirably. Thus, all subsequent fibre modifications were performed using AngströmBond®.

Although modification of the fibre ends is a significant improvement over un-modified MSFs, some issues associated with its usage were apparent. First, the MSF was still susceptible to breaking at the point where the coating has been removed, as there is nothing to protect from snapping at this point. Thus, it must be handled with care during installation. Furthermore, if the epoxy does not properly cure such that a seal is formed in the void space between the fibre and capillary, then the mobile phase can flow through the void space instead of through the fibre. This can be circumvented, however, if at only one of the fibre ends properly cured, as the uncured end can simply be placed at the detector end such that liquid is flowing out of the column instead. A more concerning issue with the modification is durability of the columns after extensive usage. While the modification initially yielded high robustness, the capillary seemed to lose its structural integrity after prolonged usage. Eventually, the capillary became very brittle and broke even under minor force. Although there is no demonstrated explanation for why this occurs, a current theory suggests that shards of silica may be present after the capillary is scored, which can scrape along the inner wall of the capillary when it is

under pressure from mobile phase flow. This potentially results in an impression along the length of the capillary which could cause it to lose its strength and consequently break.

After the non-functionalized MSFs were tested, they were subject to a sequential etching treatment using NaOH and HCl and tested a second time. In its original state, fused silica typically features a surface covered primarily by organosilicon functional groups known as siloxanes, which feature a Si-O-Si backbone and are more hydrophobic than silanols. By subjecting the column to basic solution, the siloxane moieties are converted to deprotonated silanol groups, which can then be protonated by flushing the column with a strong acid such as HCl (Figure 2.8). This treatment has been previously demonstrated to aid in exposing more silanol groups on the silica surface.[85,86] It was theorized that the increased presence of silanols along the channel walls would lead to an increase in hydrophilicity, which would translate to a more suitable stationary phase for HILIC separations.

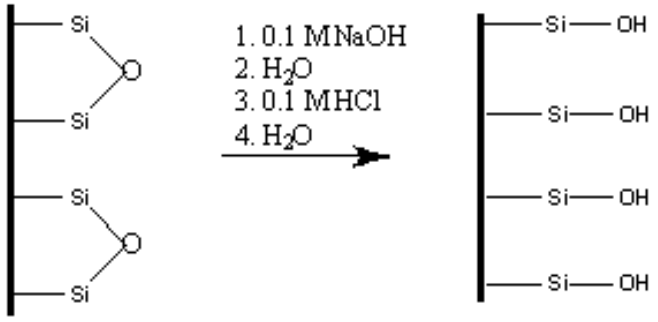

Figure 2.8: Conversion of siloxane to silanol on a silica surface. For simplicity, the hydrocarbon groups bonded to the silicon atoms are not included.

2.3.2 Hydrophilic Interaction Chromatography using non-functionalized MSFs

Appropriate selection of the mobile phase is critical in effectively performing HILIC separations. Specifically, a hydro-organic solvent mixture is necessary in order to trigger HILIC's unique retention mechanism. The organic component of the mobile phase for the majority of HILIC experiments is acetonitrile, as it expresses a high retention for most polar solutes in comparison with other organic solvents used in HILIC. Furthermore, it is an aprotic solvent and will not interfere with the aqueous layer. Although protic solvents such as methanol have been used in HILIC for certain applications, they are generally less favoured as they promote hydrogen bonding, causing them to compete with water to solvate the stationary phase surface, thus reducing the aqueous layer's ability to immobilize onto the stationary phase.[33] With these factors in mind, acetonitrile was chosen for these experiments. This decision was primarily based upon the successful use of acetonitrile in HILIC separations of purine and pyrimidine bases in the literature.[82]

The other mobile phase component for HILIC, the aqueous phase, is either pure water or a buffer solution. The pH and salt concentration of the mobile phase is important to consider as the presence of ions augments retention via ionic interactions, especially for charged species.[33] A number of different aqueous compositions were screened to determine a suitable candidate: an ammonium formate buffer was attempted at varying pH values (through the addition of formic acid). However, differences in the aqueous phase component did not produce any observable difference in the

chromatographic data, and so deionized water without any additives was used in the reported results.

An additional consideration in mobile phase preparation for HILIC is the ratio between the aqueous and organic components. A high organic phase percent (70-95%) is required in order to partition the aqueous layer from the bulk of the mobile phase. Since the aqueous component is the more strongly eluting of the two phases, a higher organic percentage will invariably generate greater retention. For the purpose of these experiments, the mobile phase was chosen to provide the greatest amount of retention possible. For HILIC, water is the most strongly eluting solvent. Therefore, 95% acetonitrile in deionized water was used in order to obtain the most retention possible while retaining HILIC functionality.

One of HILIC's strengths is its ability to retain small, polar molecules that are difficult to analyze via RP-HPLC.[2] Thus, to assess the chromatographic performance of MSFs, uracil was chosen as the analyte. Originally, a ternary mixture of purine and pyrimidine bases consisting of uracil, cytidine, and guanosine was to be analyzed using non-functionalized MSFs. However, pre-trial testing revealed that the separation of such a mixture would be too ambitious using non-functionalized MSFs. As such, the focus of the experiments was directed towards a more facile analysis of a single analyte (uracil) as a means of assessing the viability of non-functionalized MSFs as chromatographic supports.

Initial experiments were carried out using a 54-hole MSF at a length of 100 cm without any modification of the channel walls. Unfortunately, the results did not generate a typical chromatographic peak, but rather a very wide band, indicating that uracil was not being effectively retained by the column walls. Moreover, the starting time of the peak corresponded to the approximate dead volumes of the MSF, further reinforcing the notion that uracil was not being retained. A notable feature of the peaks was a gradual rise in absorbance towards the tail of the peak, with a minor absorbance spike at the very end. This characteristic suggested that some retention was present in the columns. However, based on the start times of the peaks, it is clear that the retentive mechanism must be significantly stronger in order to facilitate separation using non-functionalized MSFs.

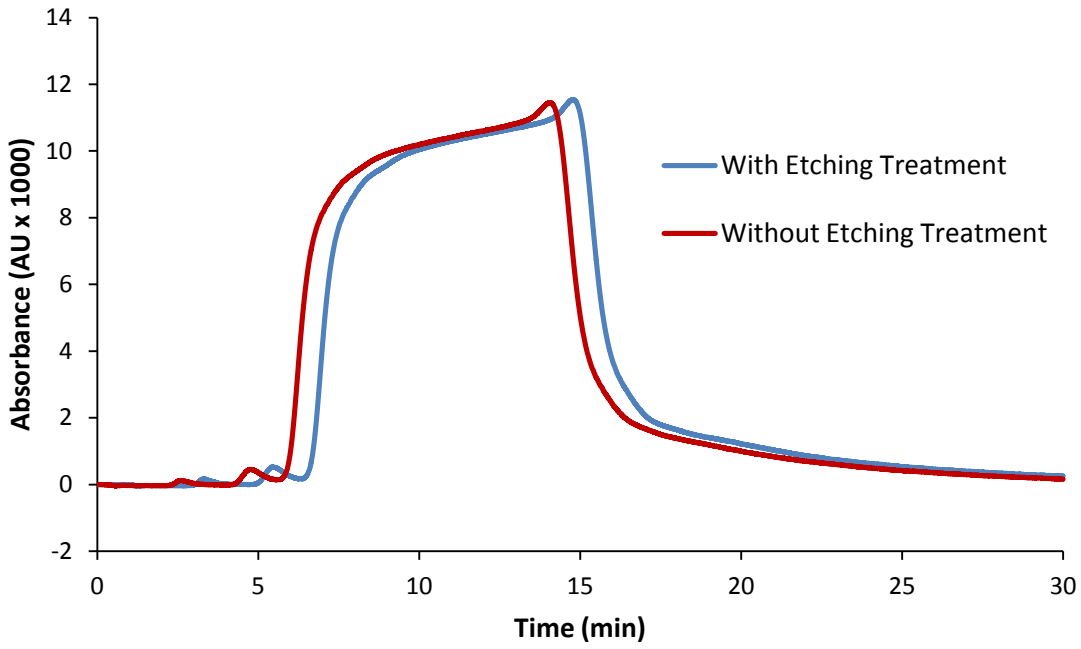

Figure 2.9: Chromatographic analysis of 5 ug/mL uracil using a non-functionalized 54-hole MSF (100 cm in length).

In an effort to enhance the separation efficiency of the column, the MSF was treated via sequential etching with NaOH followed by HCl. As explained previously, it was expected that the treatment would bolster the number of silanol groups present, thus making the channel walls more polar and enhancing its suitability as a HILIC stationary phase. However, comparison of the chromatograms obtained before and after the etching treatment did not afford any observable difference in the resulting peak, indicating that the treatment did little to alter the polarity of the stationary phase.

2.4 Conclusions

Given the poor results obtained using non-functionalized MSFs, it is clear that bare silica is inappropriate as a stationary phase for open tubular HILIC separations. The unreasonably wide peaks obtained for the analysis of uracil using MSFs in this format were indicative of an absence of retention in the column. The most obvious deduction from this is that non-functionalized silica is not polar enough to accommodate the retention mechanism. Thus, it would be necessary to functionalize the channel walls such that it expresses greater polarity. It is further likely that the surface-to-volume ratio was not large enough; perhaps non-functionalized MSFs would perform more admirably with the use of smaller channel diameters. However, MSFs with lower diameters than those found in the 54-hole MSF currently do not exist, and so this avenue currently remains unexplored.

On the other hand, the procedure used to prepare MSFs as supports for chromatography was successfully refined to afford more robust and enduring columns. Replacement of the acrylate coating at the fibre ends with a length of polyimide-coated fused silica capillary aided in preventing the column connection from being compromised due to contact with the mobile phase. The addition of capillary was further beneficial in that it simply fit better with the connections used than the acrylate-coated fibre. The primary drawback to the modification was that the capillary eventually lost its robustness, becoming brittle and eventually breaking. Nonetheless, the modified fibres were still a vast improvement over simply using the fibres directly, greatly elongating

the lifetime of the column. Thus, the modification procedure was implemented for the remainder of the fibres used in this study.

Chapter 3: Characterization of Mobile Phase Flow Inhomogeneity in MSFs using Plug Injections with UPLC

3.1 Summary of Research

The discussions brought forth in the previous chapters clearly demonstrate how differences in channel size and uniformity in multi-channel columns influence open tubular chromatographic performance. A large distribution of channel sizes will produce considerable variation in inter-channel flow velocities of the mobile phase throughout the column, which in turn diminishes separation efficiency as a result of staggered emergence of the analyte from individual channels. Given the influence that channel size distribution (or channel variance) has on multi-channel chromatography, it is necessary that measures be taken toward accurately quantifying its extent to further understand its relationship with chromatographic performance.

In the past, quantification of channel variance in MSFs has been accomplished using scanning electron microscopy (SEM), whereby cross-sectional images of a MSF is taken and, using the acquired images, the individual channel diameters are manually measured.[80,84] Unfortunately, a number of problems exist with this approach: First, only the cross-section of a MSF is considered. This generates uncertainty as the diameter of an individual channel can vary along its length, and so the diameter at a given cross-section may not be representative of the entire channel (although this can be alleviated by taking multiple SEM images along the length of the MSF, it is not desirable as it is a destructive method, requiring the MSF to be dismantled). Another concern is that

measurement of the diameter must be performed manually, which is highly subjective and can potentially lead to bias among the data. Moreover, it is impossible to perfectly position the MSF such that it is square with the imager, and so SEM images are generally taken at an angle, leading to systematically low measurements of the channel diameters. Finally, holes may not be perfectly circular (either from manufacturing imperfections or due to the fibre cutting procedure, which can skew the channel openings), in which case the measurement obtained for the "diameter" is dependent upon the angle at which it is measured. To summarize, assessment of channel variance in MSFs via SEM is a flawed technique that introduces numerous sources of uncertainty, and as such, it is necessary that a more accurate method of assessment be sought.

With this goal in mind, my research has aimed to design a novel procedure for assessing the channel variance of MSFs. This procedure seeks to determine the channel variance using a chromatographic approach through evaluation of band broadening that occurs when an LC separation is performed in the absence of a retentive mechanism. Without retention, an analyte will not stack into a tightly defined zone and instead travel through the chromatograph as an elongated plug, resulting in a very broad peak representing the analyte in the chromatogram. The width of the peak is dependent on the extent of broadening experienced by the plug. It is theorized that when such analyses are performed using multi-channel columns, the width of the analyte's band is additionally dependent upon the channel variance of the column, as dictated by the Hagen-Poiseuille equation. Thus, through analysis of the peak width for multi-channel supports with

differing degrees of channel variance, quantification of its contributing dispersive effects can be achieved.

3.2 Experimental

3.2.1 Chemicals and Materials

All aqueous samples were prepared using deionized water purchased directly from Fisher Scientific (Middletown, VA, USA). HPLC grade acetonitrile and acetone were also obtained from Fisher Scientific (Nepean, ON, Canada). Uracil was generously donated by the David Zechel group at Queen's University. AngströmBond® epoxy adhesive was purchased from The Fibre Optic Center (New Bedford, MA, USA). All chemicals were used as received.

Micro-structured fibres were purchased from various sources. The single-mode (54-hole) fibre (**1**; LMA-PM-15) and the single-mode (168-hole) fibre (**2**; LMA-20) were obtained from NKT Photonics (Birkerød, Denmark). The hollow core fibre (**3**; 32-27177), and passive air clad fibre (**4**; 320-27178) were both donated by the Institut National d'Optique (Quebec, QC, Canada). The polarization-maintaining fibre (**5**; PM-1550-01) was obtained from Thorlabs (Newton, NJ, USA). Polyimide-coated capillary columns with inner diameters (i.d.) of 30 µm (TSP030375 2), 150 µm (TSP150375 4), and 250 µm (TSP250305 6) were purchased from Polymicro Technologies (Phoenix, AZ, USA). All capillaries used had an outer diameter of 357-364 µm.

3.2.2 Scanning Electron Microscopy

Scanning electron microscopy (SEM) images of all MSFs were acquired using a Jeol JSM-840 scanning electron microscope (Tokyo, Japan). Several small pieces of each fibre (approximately 1 cm each) were cut and stripped of their acrylate coating by immersing them in acetone for approximately two minutes. The bare fibres were mounted onto an aluminum stub using masking tape, with the fibre cross-section facing upward. The fibres were gold-coated using an Anatech Hummer 6.2 Sputtering System (Hayward, CA, USA) for three minutes prior to SEM imaging. Using the SEM images, the average diameter of the channels was measured and from this data, the volumes of the MSFs were determined. Since fibre **3** did not feature circular channels, the area was estimated by subtracting the area of the circle defined by inner side of the channels from the area of the circle defined by the outer region of the channels. In addition, the relative standard deviation (RSD) of the channel diameters for each fibre was estimated. All data from SEM is given in Table 3.1. All fibres were initially insulated with an acrylate coating (not visible from the SEM images as it was removed prior to microscopy).

*Table 3.1: Characterization of MSFs via SEM. The number of channels and average diameter for **4** and **5** are separated into small and large channels. The average channel diameter for **3** was not reported as the channels are not circular.*

Fibre	***1***	***2***	***3***	***4***	***5***
# Holes	54	168	47	295 / 1	82 / 2
Average Diameter (μm)	3.8	5.6	-----	1.5 / 5.3	2.2 / 4.5
RSD (%)	1.1	1.3	6.7	11.3	16.7

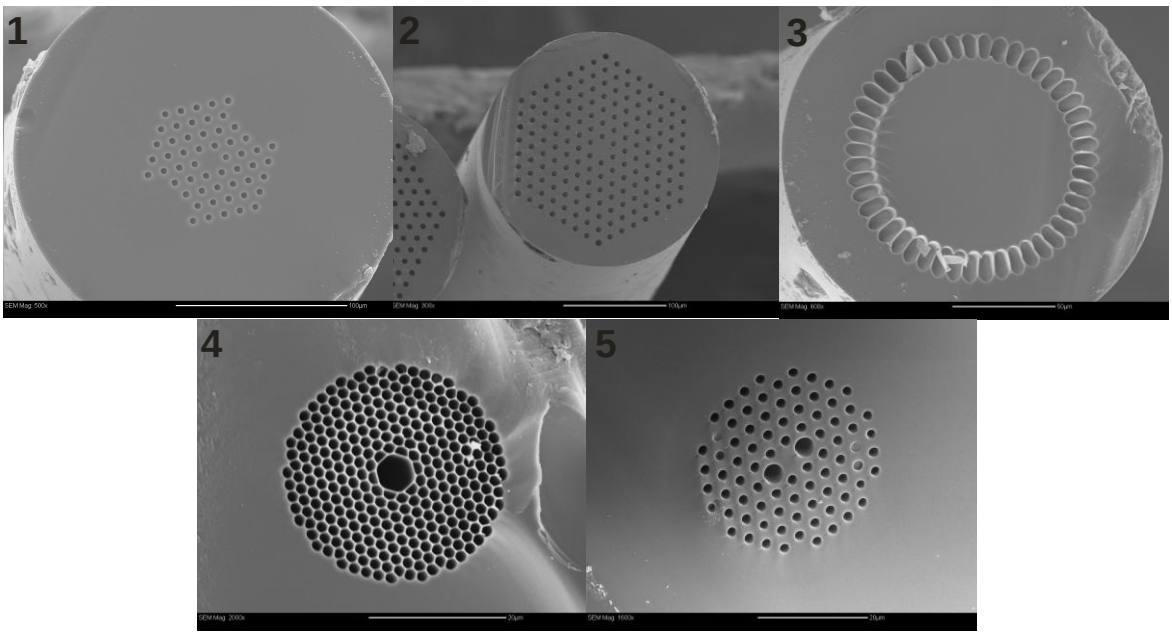

*Figure 3.1: Scanning electron micrographs of MSF cross-sections. **1**: Single-mode (54-hole) MSF. **2**: Single mode (168-hole) MSF. **3**: Passive air-clad MSF. **4**: Hollow-core MSF. **5**: Polarization-maintaining MSF. The scale bars for each image are as follows: 1: 100 µm. 2: 100 µm. 3: 50 µm. 4: 20 µm. 5: 20 µm.*

3.2.3 Preparation of MSFs

The MSFs used for the following experiments were cut using a ceramic cutter to lengths such that their internal volumes were equal. All fibres were cut to lengths corresponding to an arbitrary volume of 612 nL (which corresponds to 1 m of MSF **1**). Additional columns were prepared to lengths matching 1224 nL for MSFs **1** and **2**. A single-channel capillary column with an inner diameter (i.d.) of 30 µm (denoted ID30) was additionally prepared to serve as a control group. The lengths of all fibres and capillaries are given in Table 3.2.

Table 3.2: Estimated column lengths (cm) for MSFs and ID30 capillary normalized to a volume of 612 nL.

Column	***1***	***2***	***3***	***4***	***5***	***ID30***
Estimated Length (cm)	102	15	35	112	177	87

For all fibres, 5-8 cm of both ends were immersed in acetone for approximately 2 minutes and then the coating was manually stripped away from the fibre (except for fibre **2**, which was completely stripped of its coating). The unprotected core of the fibre was then fitted with a polyimide capillary of slightly shorter length such that about 1 cm the fibre extruded from the capillary. The core diameter for fibres **1** and **2** was approximately 240 µm and so they were fitted with an i.d. 250 µm capillary. Fibres **3-5** had core diameters of approximately 130-140 µm and were thus fitted with an i.d. 150 µm capillary. As the capillary was slid onto the MSF, the fibre core was dabbed with AngströmBond® epoxy adhesive using a wooden stir stick and constantly rotated during application to promote better coverage of the epoxy on the circumference of the core. The fibre was then placed in an oven at 100°C for two hours to allow the epoxy to cure. Afterwards, the portion of the MSF extruding from the capillary was cut to ensure that the channels were not blocked with epoxy. No other modification or treatment was applied to the MSFs before use.

3.2.4 Sample Preparation

Given the inability of underivatized MSFs to effectively retain uracil in the previous studies, it was chosen as the test analyte for the current experiments. A stock solution of 100 µg/mL was prepared in deionized water. The sample used for analysis was diluted to a final concentration of 5 µg/mL in 10% acetonitrile in deionized water. A blank sample of 10% acetonitrile in deionized water was additionally prepared.

3.2.5 Chromatography

All chromatographic experiments were performed using a Waters nanoAcquity UPLC system fitted with a tunable ultraviolet absorbance detector (Milford, MA, USA). Instrumentation was operated using MassLynx (v 4.1) software. Columns were coupled to both the detector and the injector using NanoTight unions (P-779-01) and MicroTight Fittings (F-185X), both obtained from IDEX Corporation (Oak Harbor, WA, USA). The detector wavelength was set to 260 nm for all experiments. The injection valve was equipped with a 2 µL sample loop, and full-loop injection was used to introduce samples. No temperature control was implemented.

A mobile phase of 10% acetonitrile/90% deionized water was used under isocratic conditions for all experiments. Each fibre was run a total of 15 times, divided into three trials of five runs each. After each trial, the column was removed from the chromatograph and subsequently re-installed prior to the next trial – this was carried out in order to reveal any changes in dead volume during the reinstallation of the column. Each column was tested using a flow rate of 300 nL/min. To assess reproducibility

associated with column preparation, two additional columns of MSF **2** were prepared at lengths of 15 cm and tested.

3.3 Results and Discussion

3.3.1 Preparation and Characterization of MSFs

The MSFs selected for this study were intentionally chosen to encompass a range of channel size distributions such that the procedure could be properly evaluated. Fibres **1** and **2** both feature relatively high homogeneity among their channels and were thus expected to display the least amount of dispersion due to channel variance. Fibre **3**, an air-clad optical fibre, featured a very different channel arrangement than the other fibres. Its selection was based on the fact that differences in channel sizes were easily distinguishable from the SEM image of **3**, and so it was predicted that **3** would experience greater band broadening contributions from channel variance than **1** and **2**. Fibres **4** and **5**, on the other hand, are polarization-maintaining MSFs, both of which incorporate additional larger channels (**4** has one large channel while **5** has two) among several smaller ones. This gives them a much larger RSD over the other fibres, which should translate to larger peak widths in the corresponding chromatograms. Overall, it was hypothesized that the contribution to band broadening from channel variance would increase in ascending order of the designated MSFs, with **1** and **2** producing the least broadening and **5** producing the most.

Prior to experimentation, MSFs were characterized via SEM. Cross-sectional images were taken for each fibre and, by measuring the diameters of the individual

channels, the average channel diameter was determined. From this data, the volume per unit length of each fibre was calculated, which in turn was used to estimate the lengths required to prepare the columns. The RSD of the diameters was also calculated for each MSF. This data was compared to the measured peak widths; fibres with larger RSDs among the channels are expected to feature more pronounced dispersive effects arising from channel variance. It requires mention that the data extracted from the SEM images hold a significant amount of uncertainty owing to the several drawbacks of SEM characterization mentioned previously. As such, these measurements are merely approximations which are used as estimates for column length and for comparison with the chromatographic results.

In order to measure the dispersive effects arising from channel variance in MSFs, the experiment was designed such that all other dispersive effects were held constant during analysis. In doing so, any observed differences in peak width between columns can be attributable solely to differences in channel size distribution. Dispersive effects arising from the instrument were held constant by maintaining the instrumental setup throughout the entirety of the experiment. A more pertinent source of dispersion, however, stems from longitudinal diffusion. To achieve constant diffusional dispersion between columns, it was necessary that the total volume travelled by the analyte plug was equal for all experiments. With this in mind, all fibres lengths were normalized such that their internal volumes were equal. Given the relatively wide range of volumes per unit length among the fibres tested, it was concluded that an arbitrary volume of 612 nL to which fibre lengths were normalized was appropriate. The column volume is of

further importance since band broadening from channel variance is also dependent on column volume, and its contribution becomes more pronounced as the length of the column is increased. To take advantage of this relationship, fibres **1** and **2** were additionally prepared at lengths equaling a total internal volume of 1224 nL – double the length of the original columns. These longer columns should express enhanced sensitivity to channel variance band broadening, thereby making its contribution easier to observe and measure.

The procedure for replacing the fibre ends with capillary (as detailed in Chapter 2) was again employed here. It should be noted that for these experiments, the volume of organic solvent used is miniscule, and the fibre can technically be used without modification as there is minimal contact with organic solvents that would cause the acrylate coating to swell. Nonetheless, modification of the fibre ends with capillary is still advantageous as it affords a better connection with the fittings used. Directly connecting the MSFs to the chromatograph is not ideal as the fibres, with the acrylate coating intact, have slightly smaller outer diameters which make them susceptible to slipping out of the sleeve. Moreover, the acrylate coating is fairly elastic, making it difficult for the fittings to clamp down tightly onto the fibre and keep them in place. Fitting the fibres with capillary is especially beneficial for fibres **3**-**5**, which possess very small diameters and are susceptible to snapping during use. The modification serves to heighten the robustness of these otherwise fragile columns.

No further treatments were applied after the fibres were cut and their ends fitted with capillary. As witnessed in the previous experiment regarding the use of un-modified MSFs as supports for HILIC, MSFs in their original state do not possess any significant retentive properties, which is one of the main criteria for the current experiments. Therefore, the fibres were used as is.

For comparison, a fused silica capillary column with an i.d. of 30 µm was also prepared and used as a control. Under the same chromatographic conditions, the capillaries experience similar dispersive effects as the fibres. However, since the capillaries feature a single channel, the dispersive effects of the corresponding experiments do not include any contribution from channel variance. Thus, by subtracting the plug widths derived from the capillaries from those resulting from the multi-channel supports, it was hypothesized that the dispersive contribution arising from channel variance could be distinguished.

3.3.2 Characterization of Injection Plug and Optimization of Chromatographic Parameters

The flow regime of a fluid in motion is dependent upon the ratio of inertial forces to viscous forces that characterize the fluid – this ratio is defined as the Reynolds number (R_e).[87] For a fluid travelling through a cylindrical support, R_e is calculated as follows:

$$R_e = \frac{\rho Q D}{\eta A} \quad (13)$$

where:

- ρ = fluid density
- Q = volumetric flow rate
- D = channel diameter
- η = dynamic viscosity
- A = cross-sectional area

Low R_e values correspond to a prevalence of viscous forces, which in turn cause the fluid to adopt a smooth, stable flow regime with minimal lateral mixing due to turbulence; this regime is known as laminar flow. Conversely, larger R_e values display a dominance of inertial forces, giving rise to a more unstable flow profiles marked with various eddies and vortices known as turbulent flow. It can be deduced from Equation 3.1 that, for low flow rates and dimensions, low R_e values are established and laminar flow will dominate. Thus, the experiments conducted in this study are all assumed to feature laminar flow owing to the miniaturized channel dimensions of the fibres as well as the low flow rates applied.

The presence of laminar flow in these experiments causes the analyte plugs injected into the system to assume a parabolic flow profile as they travel through the column.[88] Consequently, the analyte peak in the resulting chromatogram features characteristic distortions at the front and tail of the absorbance band (Figure 3.2). These distortions present a challenge in attempting to determine the times at which the peak starts and ends (i.e. the width of the analyte plug) – this is primarily due to the presence

of extensive tailing that make the end of the plug difficult to accurately identify (conversely, the front of the peak exhibits a very sharp initial rise in absorbance, making elucidation of the peak head comparatively easy). Measurement of the peak end is further confounded by the fact that the extent of tailing decreases considerably with decreasing channel diameters as a result of less developed parabolic flow.[88] Thus, fibres with significant differences in average channel diameter will express differences in peak width resulting from parabolic flow, which in turn makes comparing other dispersive effects (e.g. channel variance) difficult.

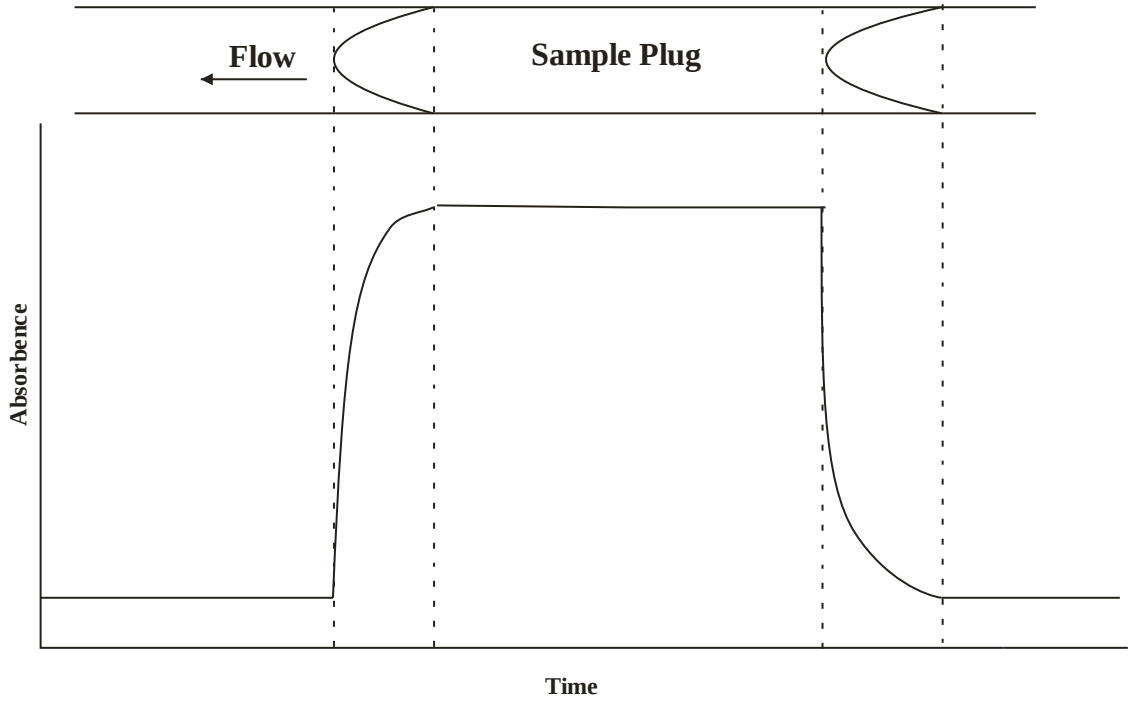

Figure 3.2: Schematic representation of a parabolic flow profile assumed by a sample plug travelling through a cylindrical support. The parabolic shapes at the front and tail of the plug correspond to the distortions observed in the absorbance peak.

To reduce tailing and other distortions throughout the peaks, the chromatographic parameters were optimized to ensure a highly uniform peak shape. The primary factors considered were the mobile phase composition and the applied flow rate. To minimize retention arising from non-covalent interaction between uracil and the silica walls, a strongly eluting mobile phase with a 90% aqueous component was implemented. It should be noted that, upon comparing this mobile phase with those of lesser eluting strengths, very little difference in the start and end of the peak was noted, suggesting that retention in the column was minimal. However, the more weakly eluting mobile phases did express more skewed peaks that favoured the tail end of the peak, which was undesirable. 90% aqueous mobile phase did not feature any such distortions, and it was therefore chosen as the mobile phase.

With respect to flow rate, although the channel variance contribution to band broadening is independent of flow rate, the extent of longitudinal diffusion throughout the column is related to the flow rate. As witnessed through the B term in the van Deemter equation, diffusional band broadening is inversely proportional to the flow velocity, and thus, higher flow rates serve to reduce diffusion, which consequently weights more significance on the dispersive effects of channel variance. With this factor in mind, a flow rate of 300 nL/min was decided upon. Flow rates appreciably higher than 300 nL/min were found to be problematic with longer columns as the upper pressure limit of the instrument was surpassed.

Using the optimized chromatographic parameters, a very uniform peak shape with minimal distortion was achieved (Figure 3.3). However, the continued persistence of tailing at the end of the peaks remained an issue when attempting to measure the peak width. As such, a protocol for measuring the width was introduced. Using this protocol, measurement of the peak width was performed by selecting arbitrary absorbance values at the beginning and end of the peak and measuring the time interval between them. For the front end, the absorbance cut-off was selected to be 500 AU. This was a fairly low value but nonetheless acceptable owing to the initial sharp increase in absorbance that occurred at the peak front. The end of the peak, by contrast, was more complicated as a result of pronounced tailing, and so the absorbance value was chosen to be sufficiently high so that it wouldn't be appreciably affected by this. It was determined that an absorbance value of 3,000 AU was sufficiently high enough that it was not significantly elongated by tailing. The times corresponding to these absorbance values were determined by referring to the chromatogram list.

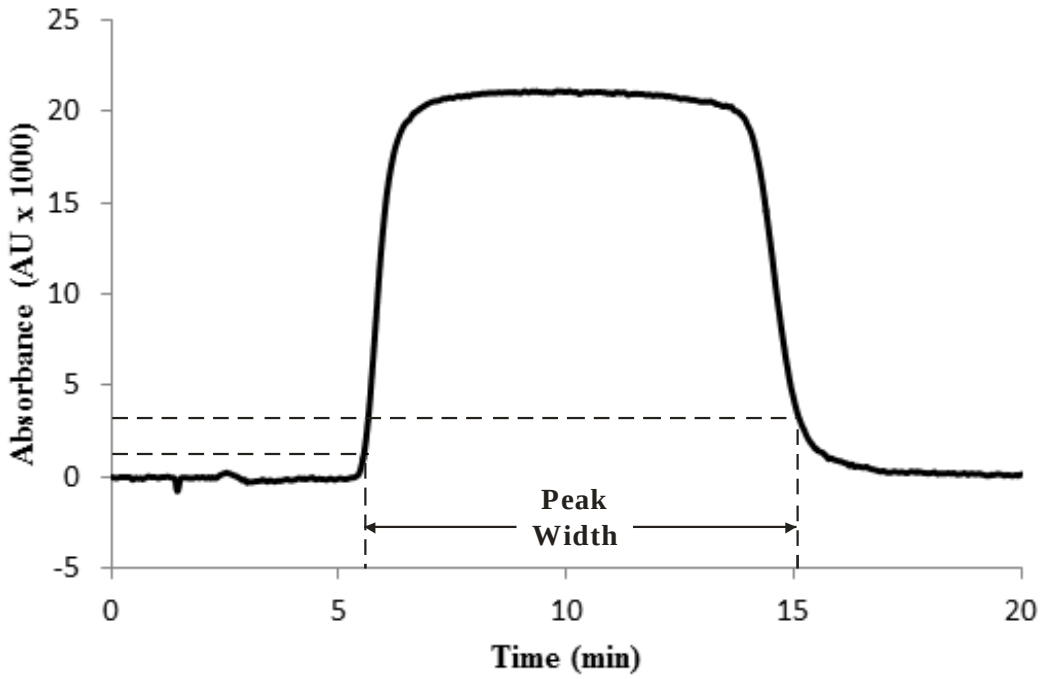

Figure 3.3: Analysis of 10 µg/mL uracil using MSF 2 at 15 cm (612 nL). The mobile phase was 10% acetonitrile in deionized water. The flow rate was 300 nL/min. Peak front was measured at 500 AU and peak tail was measured at 3000 AU.

An additional aspect influencing the peak shape is the concentration of analyte used. Experimentation with a range of concentrations of uracil was initially tested. It was discovered that higher concentrations are accompanied by more prevalent peak distortions, rendering the width difficult to assess compared with lower concentration. This observation was attributed to the effect of molar concentration on osmotic pressure, whereby larger solute concentrations lead to more pronounced diffusion. As such, minimal concentrations of analyte were applied for peak width assessment. It was determined that 5 µg/mL samples of uracil were sufficient to provide peaks with minimal peak distortion.

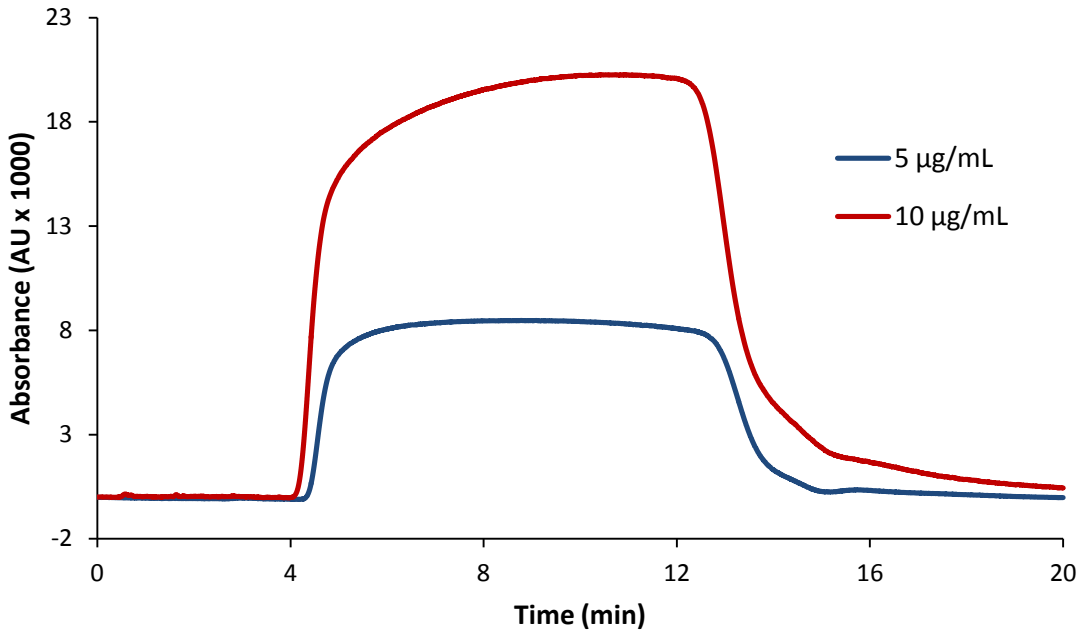

Figure 3.4: Comparison of 5 µg/mL and 10 µg/mL uracil at 300 nL/min using an ID30 capillary of 85 cm length.

3.3.3 Reproducibility of Analyte Peaks

Peak acquisition of uracil was performed a total of 15 times for each fibre. The runs were divided into three separate trials of five consecutive runs; after each trial, the column was removed and subsequently re-installed prior to performing the next set. The purpose of removing and replacing the column was to determine how the dead volume introduced at the connections between the column and the rest of the instrument affected the resulting peak widths. The data collected for fibre **2** is given in Table 3.3. It can be observed from the data that, for runs performed in the same trial (i.e. consecutively without re-positioning the column), very high reproducibility was attained. By contrast, data acquired from separate trials yielded appreciable differences in the peak width. Experiments using the other fibres expressed the same trend. The result signifies that an

indeterminate dead volume is introduced at the connections between the column and instrument during installation. Unfortunately, the amount of dead volume cannot be held constant between columns, and so it is a major source of uncertainty in the determination of peak width.

*Table 3.3: Measurement of peak widths for 15 cm column prepared from fibre **2**.*

	Peak width (min)		
	Trial A	*Trial B*	*Trial C*
1	9.685	9.781	9.706
2	9.674	9.757	9.725
3	9.667	9.765	9.715
4	9.671	9.747	9.722
5	9.658	9.751	9.723
Average	**9.671 ± 0.011**	**9.760 ± 0.015**	**9.723 ± 0.008**
Trial Average	**9.72 ± 0.04**		

Assessment of reproducibility regarding the preparation of fibres was additionally performed. Since channels can vary in size and shape along the length of a fibre, it was speculated that differences in peak width may be possible for identically prepared fibres. Furthermore, discrepancies at the fibre ends could arise from the cut of the fibre, which could lead to further differences. To assess uncertainty in the lengths of the fibres tested, two additional columns were prepared from fibre **2** at 15 cm. Only fibre **2** was selected as it features the largest volume-to-length ratio, and so any minor difference in fibre length would be most pronounced for this fibre. As before, the fibres

were performed in three trials of five consecutive runs, with the column re-positioned after each trial. The averages of each trial for all three fibres are given in Table 3.4. It was observed, however, that the uncertainty generated from differences in dead volume strongly outweighed any differences in peak width arising from discrepancies between fibres. As such, differences in prepared fibre length were not further considered for the remainder of the study.

*Table 3.4: Comparison of peak widths from three separate 15 cm columns prepared from fibre **2**. The reported peak widths are the average of the average peak widths measured for each trial.*

	Peak width (min)		
	Fibre 1	*Fibre 2*	*Fibre 3*
Trial A	9.67	9.76	9.66
Trial B	9.69	9.65	9.76
Trial C	9.73	9.72	9.62
Average	**9.70 ± 0.03**	**9.71 ± 0.05**	**9.68 ± 0.07**

3.3.4 Analysis of Channel Variance in MSFs

Following assessment of the reproducibility of the procedure, the remainder of the fibres were investigated. As before, each fibre was run a total of 15 times, with the column being re-positioned after each trial. The peak width for each fibre was reported as the average of the average peak widths calculated for each of the three trials. The results for all columns tested are given in Table 3.5. A range of peak widths was recorded for the fibres investigated. Overall, the results were in agreement with the

predictions established prior to experimentation, with **1** displaying the smallest peak width (excluding the capillary) and **5** exhibiting the largest.

Table 3.5: Peak widths obtained for MSFs with the ID30 capillary included for comparison. The ID30 value was subtracted from those for the fibres to obtain Δ CV.

	ID30	***1***	***2***	***3***	***4***	***5***
Average Peak Width (min)	9.11	9.28	9.72	9.58	11.55	13.43
Δ CV (min)	-----	0.17	0.65	0.47	2.44	4.32
±	0.05	0.07	0.05	0.06	0.11	0.09

An exception to the predictions was **3**, which unexpectedly generated narrower peaks than **2**, despite having a larger RSD for the channel diameters. This discrepancy can likely be accounted for by the fact that **3** features non-cylindrical channels, which imposes a number of flow-based consequences regarding these experiments. First, the channel geometry makes assessment of the cross-sectional areas from SEM difficult as there is no true diameter that can be measured. As a compromise, the channel area was estimated by subtracting the area of the core from the area of the circle dictated by the outer rims of the channels, while the lengths of the channels were used to estimate the RSD. Unfortunately, both estimations leave much room for uncertainty, making these measurements unreliable. Measurements for **3** were further confounded since a flat cross-section of the MSF was not achievable due to the circular arrangement of the channels – this caused the fibre to snap during cutting in such a way that the center of the fibre extruded past the outer region, making it impossible to clearly distinguish the

edge of the channels. A second consequence pertains to the applicability of the Hagen-Poiseuille equation, which describes fluid flow through cylindrical channels. Since **3** features non-cylindrical channels, the flow dynamics do not theoretically apply to the H-P equation, which further generates uncertainty since this equation serves as the premise for these experiments. Finally, parabolic flow will potentially develop differently in non-cylindrical channels, which further complicates matters in terms of peak shape and especially tailing. This was evidenced by the peaks obtained using these columns, which were highly uniform and suggested that parabolic flow is significantly less present in these fibres. Upon considering these factors, it was deemed appropriate that **3** be removed from further discussions.

To further elucidate the influence of channel variance on the peak widths, the fibres were compared to the results obtained from the ID30 capillary. As expected, the capillary expressed the smallest peak width owing to its single channel, which dismisses dispersive contributions from channel variance. The results for all fibres were compared with the peak width derived for the single channel capillary. It was theorized that, since the capillary consists of only one channel, it would experience the same dispersive effects as the fibres with the exception of channel variance. Thus, subtracting it from the peak widths of the fibres would reveal the channel variance contribution to band broadening. This value was termed "Δ Channel Variance" (or ΔCV). Plotting ΔCV against the RSD of the channel diameters (estimated from the SEM images) for fibres **1**, **2**, **4**, and **5** afforded a strong correlation. This comparison should be approached with skepticism, however, due to significant difference in the diameter of the capillary (30

µm) compared with the average diameter of the fibres, which fall in the range of 2.5-6 µm. Since the capillary channel is much larger, the analyte plug develops a more pronounced parabolic flow, resulting in extensive distortions at the front and, more importantly, the tail of the peak, making its contribution to the overall peak width more significant than for the MSFs. As such, the inability to maintain consistency in non-channel variance dispersive effects among the capillary and the fibre calls the validity of this comparison into question. In theory, the use of a single channel capillary with a smaller bore diameter would resolve this. However, the next smallest bore diameter is 10 µm, which would require a length of 780 cm to reach an internal volume of 612 nL. Such a column would be too long to use with the current setup as it would lead to pressures that exceed the instrument's threshold.

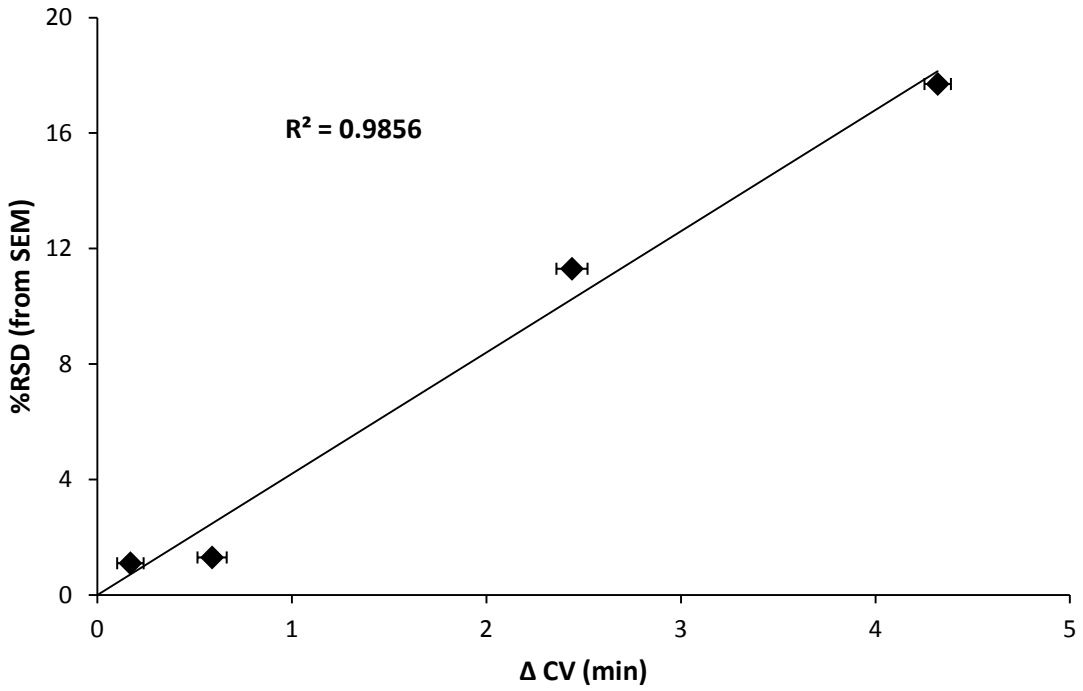

Figure 3.5: Correlation plot between Δ CV and RSD of channel diameters determined from SEM. Fibre 3 was not included.

Interestingly, the peaks for fibres **4** and **5** assume very unique profiles that afford additional information regarding the size distribution of channels in the columns. Unlike the conventional band-like peaks afforded by the other fibres (as witnessed in Figure 3.3), the profiles for **4** and **5** feature two separate increases in absorbance, which are representative of the substantial difference in diameter between the large central channels and the multiple smaller channels for these fibres (Figure 3.6). The first rise in absorbance is attributable to the emergence of the analyte from the larger channel(s). The second increase in absorbance, which occurs nearly five minutes after the first, results from the slower flow velocities that occur in the smaller channels. This pattern is reciprocated at the end of the peak, with an initial drop in absorbance shortly followed

by a larger drop. These observations are in accordance with the Hagen-Poiseuille equation, which asserts that the flow velocity in larger channels will be greater. Furthermore, the magnitude of absorbance for each is representative of the volume of analyte that flows through each of the channels – the large channel features a smaller jump in absorbance as there is a smaller volume of analyte as opposed to the sum of the smaller channels.

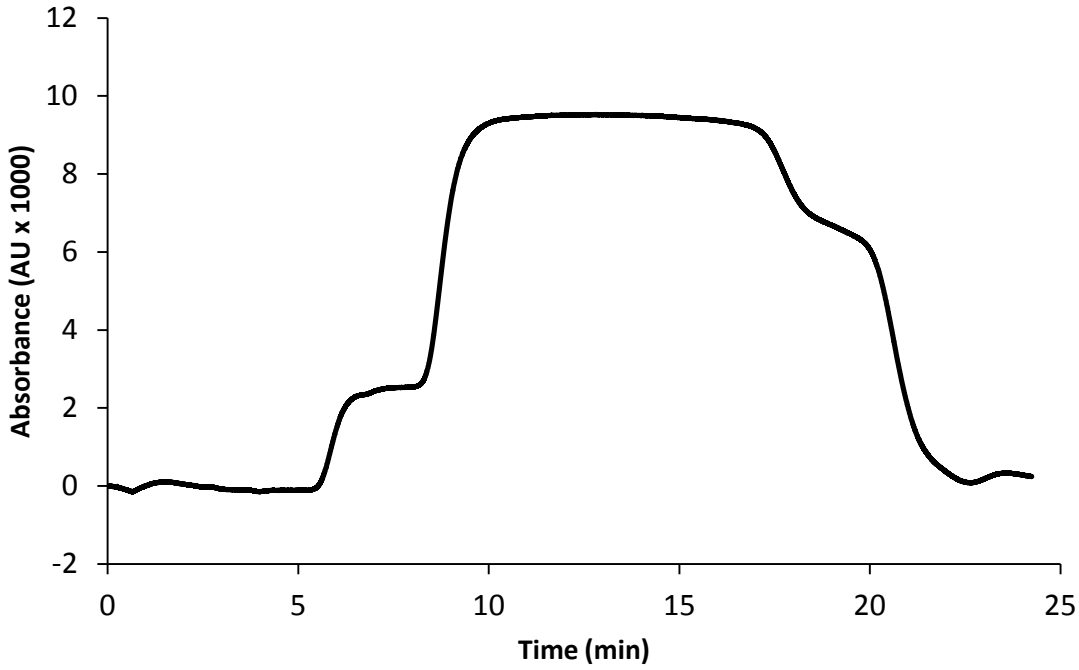

Figure 3.6: Analysis of 5 µg/mL uracil using fibre 5 at a length of 177 cm.

It was mentioned previously that dispersive effects arising from channel variance are dependent upon the length (more specifically, the volume) of the column, with the contribution increasing as the length is increased. This occurs as there is more distance which the plug must travel, leading to greater differences in emergence from the channels. Thus, in an effort to enhance the sensitivity of channel variance assessment, the procedure was applied to columns prepared at 1224 nL – double the volume of the original experiments. Only **1** and **2** were used to prepare columns for this study as they provided very little difference in ΔCV for the previous experiments, and so it was hoped that the use of longer columns would provide a greater difference in peak width between the two (**4** and **5**, by contrast, already expressed large difference in peak width, and so they were not considered here). Originally, the experiment was to be performed identically to the previous experiments in order to draw comparisons in terms of sensitivity. However, **1** could not be run at a flow rate of 300 nL/min at this length due to pressure limitations, and so the flow rate was reduced to 200 nL/min. **2** was performed at both 200 nL/min and 300 nL/min. Unfortunately, even at 200 nL/min, the use of **1** was still difficult, and after several attempts, only one trial was successfully performed. As such, the column was only performed five times, and error analysis pertaining to dead volume was not accomplished. The results are given in Table 3.6.

*Table 3.6: Peak widths recorded for columns **1** and **2** prepared at lengths corresponding to internal volumes of 1224 nL. Results are given for flow rate of 200 nL/min and 300 nL/min.*

	200 nL/min			**300 nL/min**	
	1	***2***	***ID30***	***2***	***ID30***
Average Peak Width (min)	15.67	17.17	14.12	15.23	11.08
Δ CV (min)	1.55	3.05	-----	4.15	-----

Several conclusions can be drawn from the results of these experiments. First, at 300 nL/min the ΔCV measured for **2** is significantly larger for the 1224 nL column than for the 612 nL column, which demonstrates that channel variance dispersive effects are indeed dependent on column length. Second, from the comparison of **1** and **2** at doubled length performed at 200 nL/min, a more pronounced difference in ΔCV between the two columns was observed at column volumes of 1224 nL. It must be noted, however, that the increase in column volume also carries with it an increase in the extent of distortions throughout the peak, which make width assessment less reliable due to the increased presence of tailing. These distortions are further amplified by the reduction of the flow rate to 200 nL/min, which increases the extent of diffusion present in the analysis. Despite these considerations, it is nonetheless expected that these contributions are accounted for through comparison with the results obtained from the ID30 column at 1224 nL volume.

3.4 Conclusions

To summarize, a novel procedure for characterizing mobile phase flow inhomogeneity in MSFs was successfully conceived. It was demonstrated from the experiments conducted that, in the absence of retention, peaks widths of the resulting chromatograms were dependent upon the extent of channel variance for multi-channel columns. This observation was further reinforced by the correlation revealed between the peak widths extracted from the fibres and the RSD of the fibre channels. Moreover, the peaks acquired for separations performed using hollow-core and polarization-maintaining MSFs, which additionally feature large channels among several smaller ones, express unique shapes that are characteristic of the column geometry.

A number of outstanding issues exist with the method in its current format. Although the method outlines clear differences in peak width for fibres with large channel distribution, poor precision owing to uncertainty from dead volume at the connections is a primary source of uncertainty as it cannot currently be held consistent between separate installments of the columns. Furthermore, the measured fibre lengths are approximate due to the nature of their acquisition, which was through measurement of channel diameters via SEM. As such, the internal volumes of each fibre are likely not equal, generating additional uncertainty in the results. Another issue is the measurement protocol applied in assessing the width of the peaks. Although the introduction of this protocol was to address tailing at the end of the peaks, the differences in peak shapes for each fibre suggest that this approach may not be entirely accurate. Finally, comparison

with a single channel capillary is not realizable currently, a result of differences in the development of parabolic flow for analyte plugs travelling through channel of different diameters. Without such a comparison, it is impossible to attribute the fraction of the peak width that stems from channel variance.

Despite the drawbacks of the procedure, it is nonetheless a strong initial effort that stands as a proof of principle that the dispersive effects of channel variation in multi-channel columns can be characterized in this regard. With the eventual resolution of the current issues, it is believed that this method will provide a significant step towards the development of OTLC.

Chapter 4: Characterization of Mobile Phase Flow Inhomogeneity in Multi-channel Supports using Computational Fluid Dynamics

4.1 Summary of Research

Computational fluid dynamics (CFD) is a subset of fluid mechanics that concerns the application of numerical analysis and algorithms as a means of solving problems concerning fluid dynamics. Given the complexity of the majority of such numerical methods, which often cannot be feasibly performed manually, CFD relies heavily on the use of computer processing to calculate solutions through successive iterations in a timely manner. As the processing power of computers continues to grow, a greater range of fluidic problems with increasing complexity can be solved with increased accuracy, precision, and speed. Currently, CFD features a diversity of applications in chemical engineering and research,[89] which has extended into fields such as microfluidics,[90] and fuel cells.[91]

The process of solving fluid flow problems through CFD is divided into several successive steps. First, the geometry of the fluidic structure is designed and the corresponding boundary conditions (namely, the inlets, outlets, and walls) are defined. Following this, the volume through which the fluid is to travel is divided into numerous discrete cells (or elements) for which numerical iterations are individually performed. These cells are collectively referred to as the mesh. The number of cells comprising the mesh for a given geometry will influence the quality of the solution, with more cells affording solutions with higher precision and accuracy. However, the gain in quality

comes at the expense of analysis time, as the increase in cells will lead to more calculations which must be performed. More complex meshing may even require greater processing power, which further deters the use of finer meshing. Once the mesh is set, a simulation is run whereby the flow properties in each individual cell are iteratively calculated until it converges to a single solution. CFD calculations are primarily based on the Navier-Stokes equations, a collection of formulas derived from the application of Newton's second law to fluid flow.[92] Following the simulation, post-processing of the data occurs and conclusions are drawn.

To supplement the results obtained from the characterization of mobile phase flow velocity distribution in MSFs (Chapter 3), CFD was introduced to model fluid flow through multi-channel supports. With CFD software, simplified columns possessing multiple channels were virtually constructed, and the channel sizes were tailored to model the channel variance expressed in MSFs. Using these channels, a pulsed injection of a solute was simulated and differences in flow velocity among the channels were analyzed. It was hoped that a computational examination of fluid flow in this regard could serve as a point of comparison with the chromatographic experiments used to assess channel variance in MSFs.

4.2 Experimental

4.2.1 Materials

CFD simulations were performed using ANSYS Engineering Simulation Software (v 13.0), obtained from CMC Microsystems (Kingston, ON, Canada). Specifically, the ANSYS Fluent analysis system was used. The software was operated using a personal computer with Microsoft Windows 7 Home Premium 2009 (service pack 1, 64-bit), an Intel Core i7-2600 processor (3.40 GHz), and 8.00 GB of RAM. Microsoft Visual C++ Express was used for writing and compiling user-defined functions (UDFs). Windows SDK 7.1 Command Prompt was used to incorporate the UDFs into the ANSYS compilation environment.

4.2.2 Pre-simulation Processing

All geometries used for CFD simulations were designed using ANSYS DesignModeler. The geometries were constructed in three dimensional space. As an initial trial, a simplified multi-channel column comprised of two channels was constructed. The channel diameters were set to 5 µm and 6 µm, and the channel lengths were set to 500 µm. Later trials were performed using geometries with channel lengths of 1000 µm, 2500 µm, and 5000 µm were additionally constructed. The channels were joined at the front of the column by a larger "injection channel," which served as the point of introduction for fluid entering the column. The injection channel was designed with a diameter of 14 µm and a length of 10 µm. The geometry for the two-channel column is illustrated in Figure 4.1.

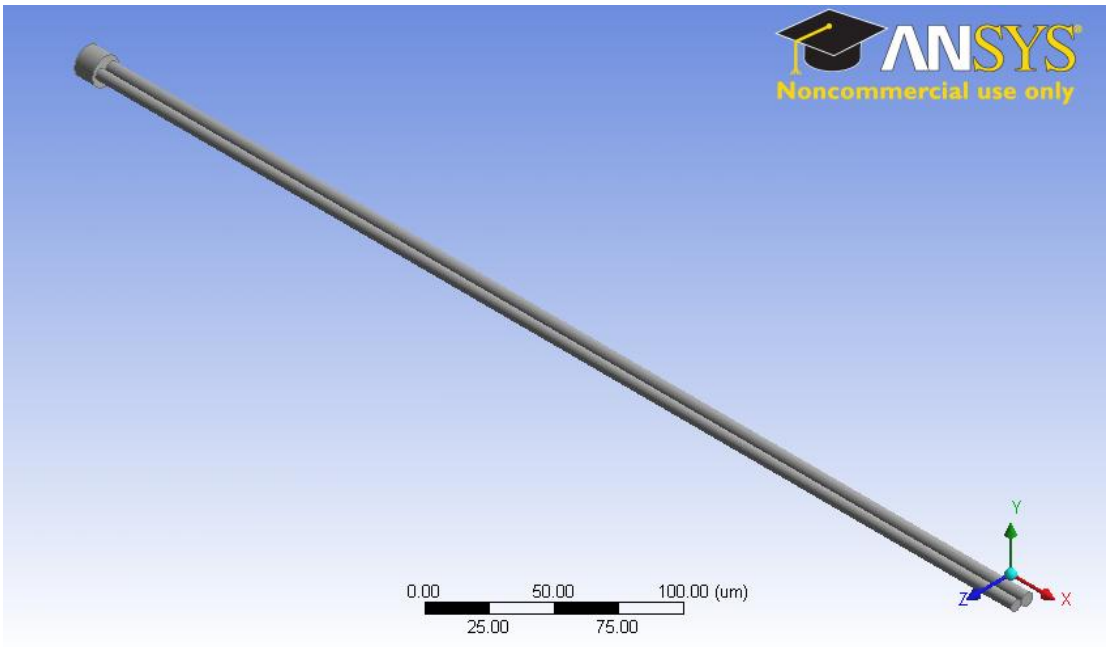

Figure 4.1: Isometric view of a two-channel column designed using ANSYS DesignModeler. The injection tube is located in the top left corner. The leftmost channel is 5 μm while the rightmost channel is 6 μm.

Following construction of the channel geometry, the boundary conditions were then established. The front of the injection tube was set as a "velocity" inlet, allowing the velocity of the fluid to be specified as it enters the column. The ends of the two channels were set as "pressure" outlets, and the pressure was set to 0 (indicating that the column was open to the atmosphere). The outlet for each channel was separately defined such that flow through each channel could be individually assessed. The remainder of the geometry was set as a "wall," indicating that it was an impermeable barrier to flow. The volume of the body was then defined as "fluid" to enable fluid flow simulations.

Once the geometry and boundary conditions were in place, the mesh was implemented into the flow volume. The ANSYS Meshing program was used to generate the mesh. Under the cell sizing options, the relevance center setting was set to fine, smoothing was set to high, and span angle center was set to fine. All other meshing options were left as the default setting. The mesh was then generated and exported for later use, and the ANSYS workbench was closed.

Following the initial simulations using the two-channel column, more complex columns with five channels were designed. Several five-channel columns (labelled A-E) were prepared, each possessing an average channel diameter of 5 μm. The columns differed in that the individual channel diameters were varied such that each column expressed different relative standard deviations (RSD) among the diameters. The channels were equidistantly spaced from the center of the column and equally spaced from each other. The channel dimensions for the five-channel columns are given in Table 4.1, and a figure of the geometry is illustrated in Figure 4.2. As before, an injection channel was placed at the head of the column; the diameter of the injection channel was expanded to 20 μm in order to accommodate the channels (the length was maintained at 10 μm). All five-channel columns were prepared at lengths of 1000 μm.

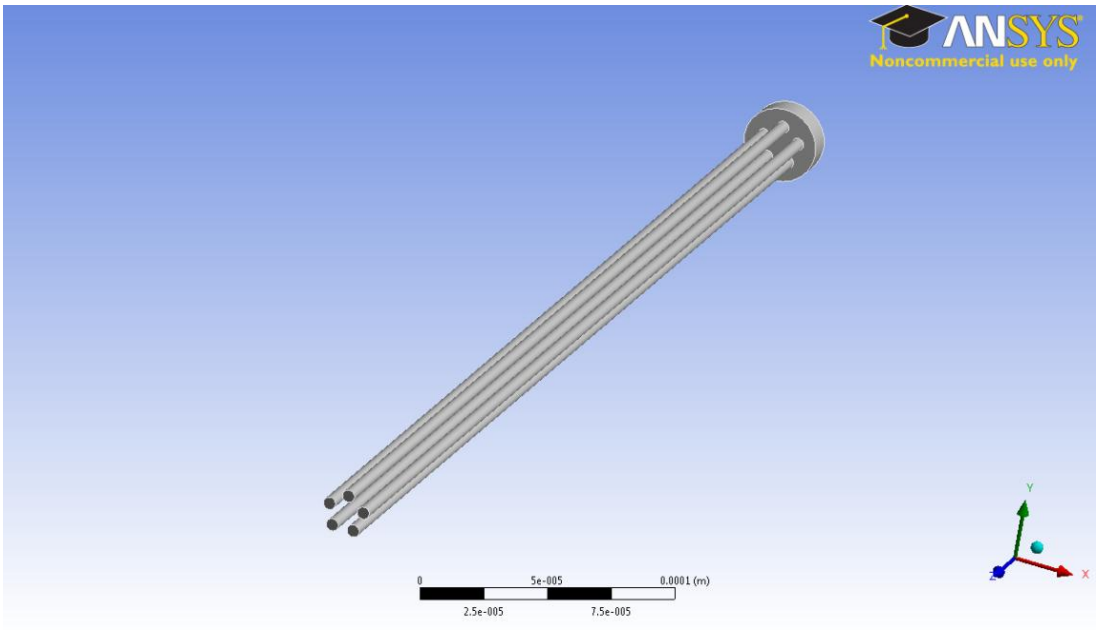

Figure 4.2: Isometric view of a five-channel column designed using ANSYS DesignModeler. All channels are 5 µm in diameter.

Table 4.1: Channel diameters used for five-channel columns. Columns were designated a letter (A-E) with each column possessing a different RSD.

	Channel Diameter (µm)				
Column	***A***	***B***	***C***	***D***	***E***
Ch. 1	5.00	4.90	4.80	4.60	4.00
Ch. 2	5.00	4.95	4.90	4.80	4.50
Ch. 3	5.00	5.00	5.00	5.00	5.00
Ch. 4	5.00	5.05	5.10	5.20	5.50
Ch. 5	5.00	5.10	5.20	5.40	6.00
Average	5.00	5.00	5.00	5.00	5.00
RSD (%)	0.00	1.58	3.16	6.32	15.81

4.2.3 CFD Simulations

CFD Simulations were performed using ANSYS Fluent, accessed using the Windows SDK 7.1 Command Prompt. A pressure-based solver with absolute velocity formulation and transient time conditions (using first-order implicit formulations) was chosen for calculations. Additional simulations were performed under steady-state time conditions to test for convergence of the numerical solutions prior to performing the transient case. The pressure-velocity coupling scheme was set to SIMPLE, and the spatial discretization parameters were left as the default settings. Neither gravitational nor temperature effects were included in the calculations. Among the various flow models available through Fluent, the viscosity and species transport models were the only two selected to dictate the flow simulation. The viscosity model was set to laminar to match the flow regime occurring in microfluidic channels. In the species transport options, inlet diffusion and diffusion energy source were both selected, and the number of components was set to two.

Under the materials settings, the channel walls were specified as fused silica so as to represent the channel walls of a MSF. The density was set to the literature value for silica, 2.20 g/cm^3.[93] The fluid used in the simulation was set as a mixture of water and acetone. The physical properties for individual liquids were first defined (the physical constants for both were directly imported from the ANSYS database). The acetone-water mixture was then defined. The physical properties of the mixture were governed through the use of fluidic mixing laws available through the Fluent software: A volume weighted mixing law was used for density and a mass-weighted law was selected for

viscosity. The mass diffusivity of the mixture was set to multicomponent and the diffusion coefficient was set to 1 x 10^{-30} m^2/s. It should be noted that this is far below the literature diffusion coefficient of acetone in water (1.14 x 10^{-5} m^2/s).[94] The coefficient was set to an artificially low value to remove diffusion from the system and simplify the simulation. The linear flow velocity of the fluid was set to 0.10 mm/s for all simulations.

To portray the experiments used to assess channel variance in MSFs, the water-acetone mixture was implemented such that the column is initially filled with water, and a pulsed injection of acetone was then introduced and its migration through the channels monitored. To accomplish this, a user-defined function (UDF) was written and incorporated into the Fluent software (the code for the UDF is given in Appendix A). The UDF was written such that a pulsed injection of acetone would enter from the inlet from time 0.5 s to 2.0 s during the simulation. Simulations performed under steady-state time conditions did not incorporate the UDF.

To observe the passage of the acetone plug through the columns, surface monitors were positioned at the inlet and the outlets using the boundary conditions previously established. The report type was set as a facet average, and the field variable of the monitors was set to "species" and specifically allocated to detect the mass fraction of acetone at the surfaces. The monitors were commanded to generate plots of the mass fraction with respect to flow time, and data was acquired for each time step. Each monitor was individually named and written. The mass fraction data was reported both separately for each channel and as a sum of the area-weighted average of the combined

channels. In addition to the placement of monitors, animations were prepared such that videos of the plug injection and subsequent migration through the channel could be obtained. For the steady-state approximation, a volume rendering of the flow velocity throughout the column was additionally generated.

Once the monitors were positioned, the initial conditions of the solution were defined (namely, the initial flow velocity was set in the appropriate direction) and a simulation was performed. For steady-state simulations, 20 iterations were used for all geometries. For transient time conditions, the time step size was 0.05 s with a maximum of 20 iterations per time step. The number of time steps varied depending on the simulation – a sufficient amount of time steps was chosen to ensure the plug had fully traversed through column prior to the end of the simulation. The reporting interval and profile update interval were both set to one (the default setting).

4.3 Results and Discussion

4.3.1 Geometry and Mesh

To demonstrate that flow velocity inhomogeneity in multi-channel columns could be modelled using CFD, a simple column containing two channels was devised as an initial demonstration. The two channels were designed to have an appreciably large difference in channel diameters such that a difference in flow velocity between the two could be easily distinguished. It was determined through pre-trial simulations using the two-channel geometry that a difference of 1 μm between the channel diameters (5 μm for one and 6 μm for the other) was sufficient to generate an observable difference in

flow velocity among the channels. Following this proof-of-principle experiment, more elaborate columns were prepared to better exemplify the flow profiles observed in multi-channel supports such as MSFs. These columns all featured five channels and possessed an average channel diameter of 5 μm. The individual channel diameters were varied for each column so that a range of RSDs were observed among the columns.

In addition to the number and diameter of the channels, other dimensions also played an important role in the overall column design. To simplify injection such that it arose from a single source, the channels were adjoined at the front of the column by a larger "injection channel". The head of the injection channel served at the inlet source for fluid entering the column. The use of this channel not only simplified injection by providing a singular inlet source (as opposed to separately defining inlet sources for each channel), but also served to model the actual chromatographic experiments conducted with MSFs (Chapter 3), whereby the source of the analyte was from a single-channel capillary. It was additionally important to consider the positioning of the channels; to ensure that the initial velocity of the fluid entering each channel was consistent, the channels were equidistantly spaced from the center of the column and equally spaced from each other. This was rationalized by the fact that, under laminar flow conditions, the flow velocity will be faster in the center of the column than near the channel walls.

For initial trials involving the two-channel column, the channel lengths were set to 500 μm. It should be noted that this is significantly shorter than the column lengths

used during the characterization experiments of MSFs, which featured lengths in the centimeter scale. It was originally envisioned that column lengths on a scale that was comparable to the MSFs used could be prepared using ANSYS. However, it was found that the use of longer column geometries drastically increased the time required to perform each simulation (since the mesh for these columns are comprised of more elements). As an example, it is predicted that a column of just 1 cm would take several days to complete under the current settings. As such, column lengths were limited to the micrometer scale to afford faster simulation times. Later experiments, however, were additionally performed at lengths of 1000 µm, 2500 µm, and 5000 µm in an attempt to generate a greater displacement of the arrival times of acetone among the channels. For the five-channel columns, a length of 1000 µm was decided upon.

The quality of the resulting mesh was another factor to consider when preparing geometries for CFD. A variety of options and settings were available through the ANSYS Meshing application that allowed for a highly customizable mesh. However, given the relative simplicity of the geometries employed, it was not considered necessary to stray from the software's default settings. One exception was the mesh sizing options, which were manipulated to generate a finer mesh comprised of a greater amount of cells. This change was made simply because an increased mesh quality was attainable without significantly hampering the computational speed.

4.3.2 Problem Setup

In deciding upon the settings to use for the pulsed injection simulations, the goal was to minimize the complexity of the system as much as possible so that the flow velocities among the channels could be easily observed and compared. With this in mind, only two of the available flow models were applied to the simulation; the viscous model and the species model. The viscous model was used to incorporate laminar flow into the simulation such that the fluid would flow as though it were migrating through a microfluidic channel. The species model was required to enable multiple components (i.e. water and acetone) to comprise the fluid in addition to controlling mixing and diffusion between the components of the fluid mixture. No other models were considered for the experiments conducted. The time conditions for the solver were set to transient; this was necessary due to the changing composition of the fluid entering the inlet over time, which cannot be treated under steady-state conditions.

The selection of materials used (both the fluid and the solid support) was predicated upon the intent to emulate the materials employed for the experiments pertaining to the characterization of MSF channel variance. To accomplish this, a multicomponent fluid consisting of a mixture of water and acetone was defined, with water serving as the bulk of the liquid. From a chromatographic perspective, water served as the mobile phase while acetone played the role of analyte. Acetone was chosen as a substitute for uracil, which was used in the previous experiments for the characterization of MSFs – in experimental trials, acetone was tested as a candidate for plug injections, and it was found to perform similarly to uracil. Moreover, it was easier

to import acetone from the ANSYS database instead of creating uracil (it was readily available from the database). One notable change in the physical properties of the mixture was the diffusion coefficient, which was set to an artificially low value of 1 x 10^{-30} m^2/s (see section 4.3.3 for further details). Silica was chosen as the material of the column walls so as to emulate the material composition of MSFs. However, this declaration likely had minimal impact on the results since the only property that was altered in setting the material was the density. The simulation did not incorporate chemical interactions between the fluid and the wall.

To model the experiments used to characterize fluid flow in MSFs, the simulations were designed to initiate a pulsed injection of acetone through the column at a particular time, originally filled with water. However, it was not possible to transiently alter the composition of the fluid entering the column using the ANSYS Fluent interface alone. As such, it was necessary to write a UDF capable of dictating the fluid composition over time and implement it into the software. Using the UDF, the size of the injection plug could be controlled simply by changing the size of the time interval for which acetone is to be injected. Furthermore, the time at which the plug entered the column could be set. For initial trials, the UDF was written such that from time 0 to 0.5 s, 100% water was entering the inlet. From 0.5 s to 2.0 s, 100% acetone was injected, and then back to water for the remainder of the simulation (Figure 4.3). It should be noted that at the given velocity, the time interval during which acetone was injected corresponded to a volume of just a few nanoliters – to achieve 2 μL as in the characterization experiments, a time interval of 6.7 min would be necessary. However,

given the relative small time frame of 5 seconds used for the simulation, the size of the acetone plug used for the initial trials was a necessary compromise in order to allow the entire plug to reach the end of the column.

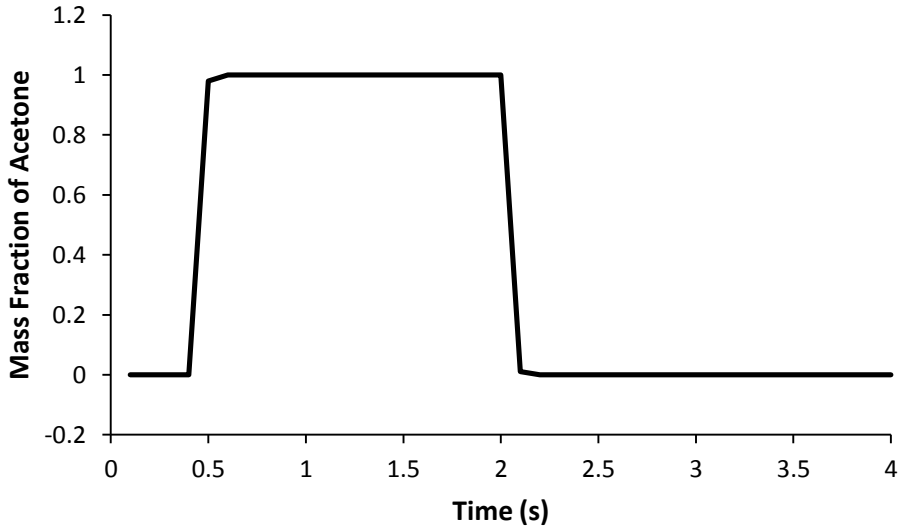

Figure 4.3: Mass fraction of acetone entering the column inlet over time.

4.3.3 CFD Simulations

Prior to performing CFD simulations under transient time conditions, a steady-state approximation was first carried out without incorporating the UDF (in other words, water was set to constantly flow through the column throughout the entirety of the simulation). For the transient simulation, numerous calculations are needed for each time step in order to converge to a solution before proceeding to the next time step. By preparing and running a steady-state approximation before the transient case, the simulation is provided with a "first-guess" solution which enables it to converge to a solution for each time step using a lesser amount of iterations. This not only serves to

reduce simulation time, but also improves the accuracy of the converged solution. From the steady-state solution, a contour diagram of the flow velocities throughout the column was generated (Figure 4.4). From the diagram, a clear difference in flow velocity was noted between the two channels, with a higher velocity observed in the 6 µm channel (in accordance with the Hagen-Poiseuille equation).

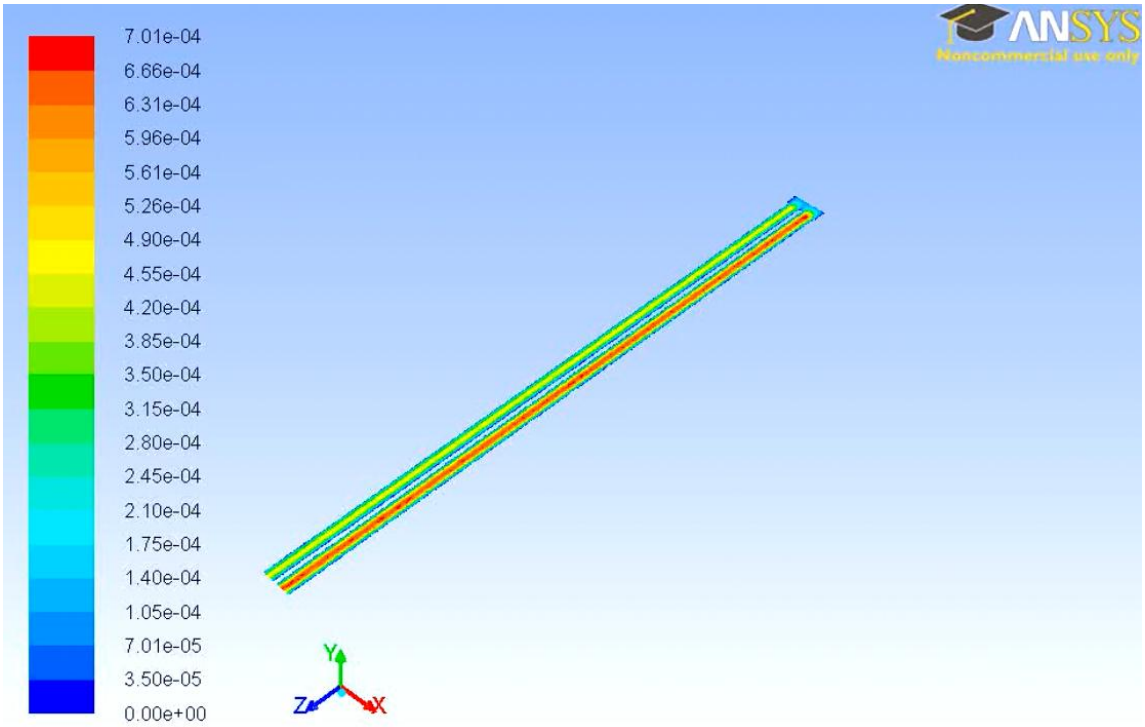

Figure 4.4: Contour diagram depicting the flow velocities for the two-channel column geometry under steady-state time conditions. The 6 µm channel is on the bottom and the 5 µm channel is on top.

A prominent issue encountered during early CFD trials using transient time conditions was that the acetone plug immediately underwent extreme diffusion upon entering the column. As a result, the tail end of the plug appeared as though it were

immobilized near the column inlet, and consequently, failed to completely reach the end of the column in a reasonable amount of time. This occurred despite the fact that the diffusion coefficient for acetone in water was set to the correct literature value (1.14 x 10^{-5} m^2/s). Several settings related to diffusion and mixing of the mixture components were adjusted in an attempt to resolve this issue, but unfortunately, the diffusion persisted and the mixture failed to behave realistically. As a compromise, the diffusion coefficient was set to an artificially low value of 1 x 10^{-30} m^2/s in an effort to remove diffusion altogether (values significantly lower would not be accepted by the program). Even using this value, diffusion was still present in the simulation. However, it now seemed to represent much more realistic diffusional behaviour. Based on this result, it was eventually decided upon to use this value for all subsequent tests. While these settings are not an accurate reflection of real microfluidic channels, the resulting simulations were nonetheless capable of elucidating flow velocity variation in the geometries prepared.

With the aforementioned settings in place, simulations detailing the transient migration of acetone through the two-channel column were once again performed. Assessment of the simulation results was carried out primarily through the generation of graphs in which the mass fraction of acetone at the channel outlets was plotted against the flow time. Given the strong resemblance of these plots with actual chromatographic data, the graphs were labelled as "pseudo-chromatograms". Pseudo-chromatograms were acquired individually for each outlet and subsequently overlaid onto a single graph for direct comparison. The graphs depicted a distinct displacement in the mass fraction

peaks for acetone at the outlets of each channel (Figure 4.5), concluding that a flow velocity distribution for multi-channel columns could indeed be computationally generated. This conclusion was further reinforced by corresponding video animations of the migration of acetone through the channel.

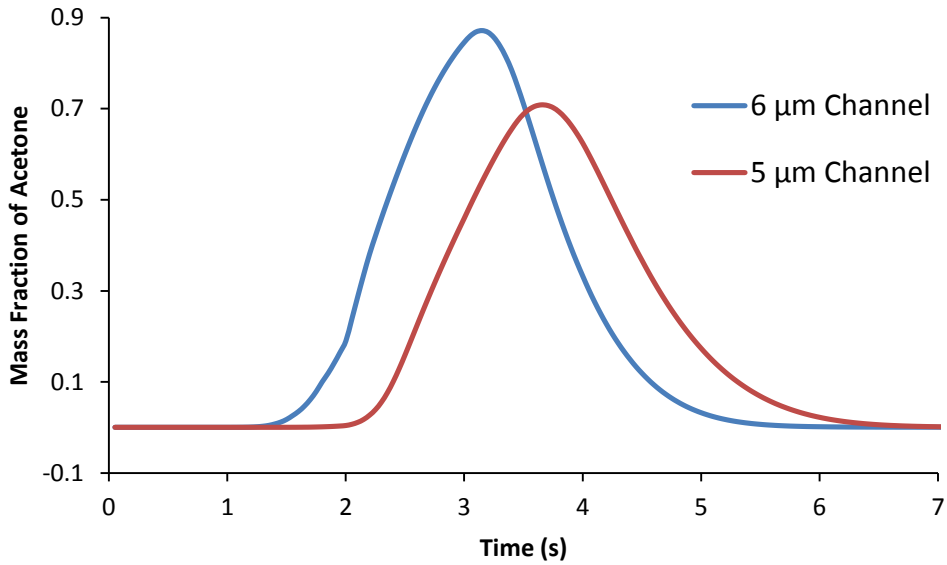

Figure 4.5: Pseudo-Chromatogram of the mass fraction of acetone at the channel outlets over time for a two-channel column.

Following the initial simulation using channel lengths of 500 µm, longer column geometries were explored with the expectation that the mass fraction peaks for the two channels would become increasingly displaced as the column was lengthened. As such, the two-channel column was additionally prepared at lengths of 1000 µm, 2500 µm, and 5000 µm. The results were quantified through measurement of the center (in time) of each peak. The peak centers were calculated by measuring the midpoint between the two times corresponding to when the mass fraction of acetone equalled 0.01. The time

difference between the peak centers of the 5 μm and 6 μm channels was then determined for each column, and the results were compared. As expected, an increase in peak width was noted as the column was lengthened (Table 4.2), reinforcing the notion that differences in flow velocities among channels are more easily detectable using longer columns. Moreover, a reasonable linear correlation was noted between the channel length and the time difference (Figure 4.6). Unfortunately, column lengths significantly greater than 5000 μm could not be explored as the mesh was too large for the computer to generate.

Table 4.2: Difference in time (s) between the peak centers of the 5 μm and 6 μm channels the for two-channel column at various lengths.

Column Length	*500 μm*	*1000 μm*	*2500 μm*	*5000 μm*
6 μm Ch. Peak Center (s)	3.40	5.50	13.45	32.65
5 μm Ch. Peak Center (s)	4.20	6.75	18.00	43.75
Difference (s)	**0.80**	**1.25**	**4.55**	**11.10**

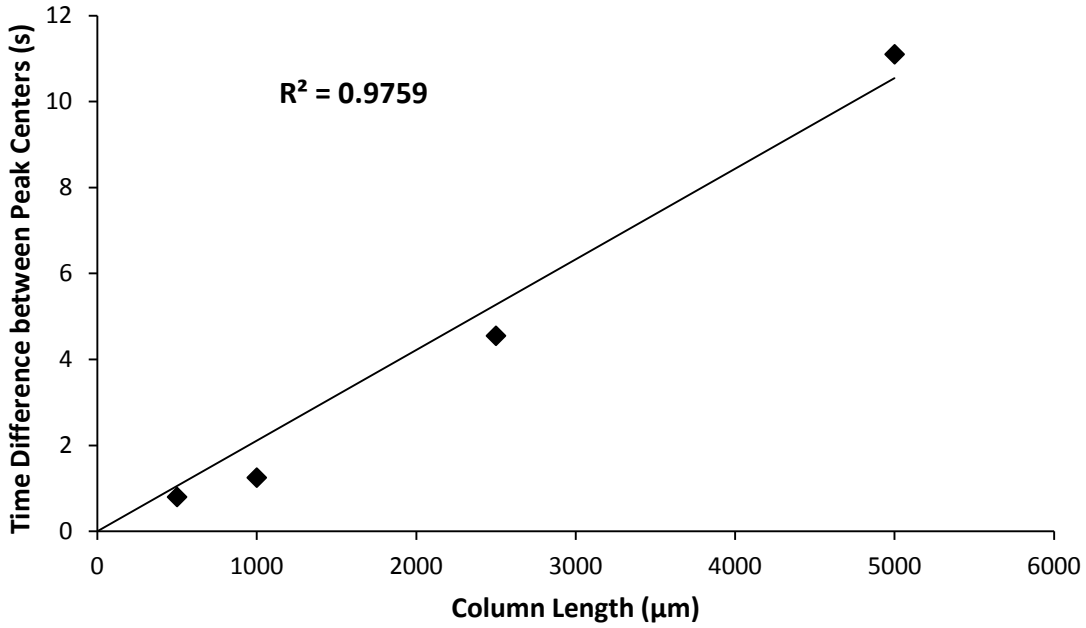

Figure 4.6: Correlation plot of displacement between peak centers of the large and small channels against the column length for the two channel column.

Despite the enhanced sensitivity with respect to peak width, some issues regarding the use of longer columns were apparent. First, the ANSYS software was unable to generate an appropriate mesh for columns significantly longer than 5000 µm (the meshing program would simply give an error and terminate the command), which limited the lengths that were possible. Currently, no method of addressing the error has been found, despite multiple attempts to adjust the settings to enable proper mesh generation. Furthermore, larger geometries invariably required a greater number of cells in the corresponding mesh in order to cover the entire fluid volume. It was found that, even with upgraded processing power supplied by the new computer, significantly more

time was needed to perform simulations involving larger columns. In the interest of time, this imposed a practical limit to the column length.

Following assessment of flow profiles in the two-channel column, efforts were directed towards characterization of the five-channel columns to explore the relationship between channel diameter RSD and flow velocity variation. To characterize the results for the columns, the area-weighted average (with respect to the outlet surfaces) was calculated for the mass fraction of acetone for each channel and subsequently added together to form a singular peak. The width of the resulting peaks were then measured using the same assessment protocol employed for the uracil peaks acquired for uracil via chromatography using MSFs, whereby the start and end times of the peaks were determined according to arbitrarily chosen mass fractions values. For these simulations, the start and end times of the peaks were both calculated at mass fraction values of 0.010. Initial testing was performed using column A (the control group), which featured equal diameters of 5 μm for all five channels. With the exception of some minor differences in the peak heights, the peaks obtained for the individual channels were nearly identical with equal start and end times (Figure 4.7), signifying that flow variation among channels is largely absent when the RSD of the channel diameters equals zero.

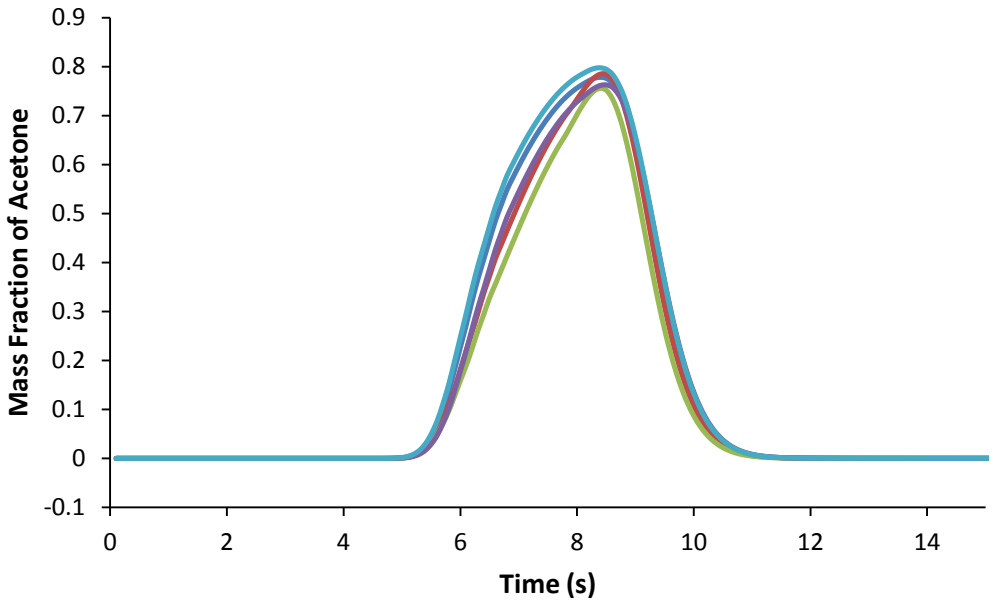

Figure 4.7: Pseudo-chromatogram of mass fraction of acetone over time for the individual channels in column A.

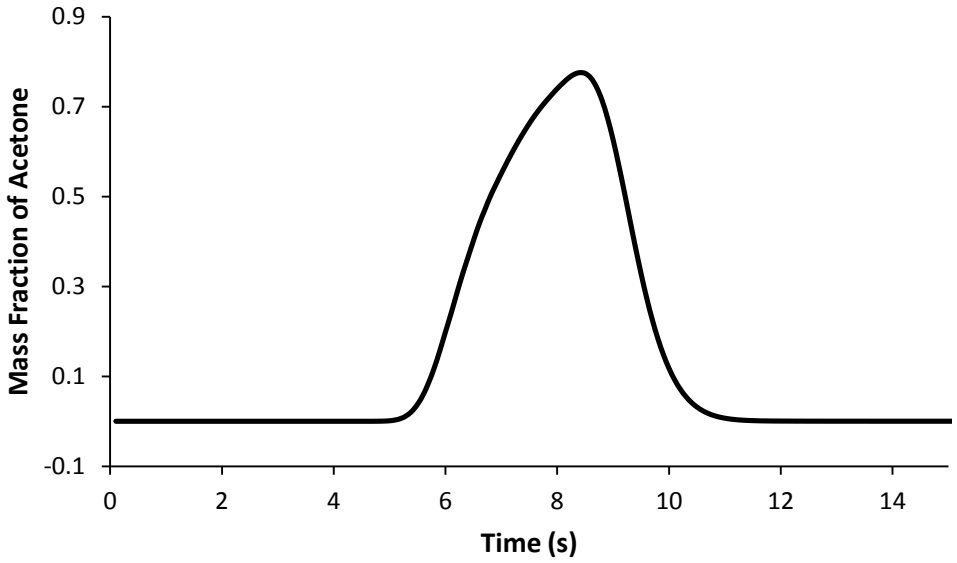

Figure 4.8: Pseudo-chromatogram of the sum of the area-weighted averages for the mass fraction of acetone over time through each channel for column A.

As the channel sizes were varied, differences in peak displacement for the individual channels became increasingly apparent, and the width of the summed peak became greater (Table 4.3; see Figure 4.9 for the results of column E). This finding was consistent with the results obtained in Chapter 3, which showed that the peak width was dependent upon the RSD of the channel diameters for a given column. Furthermore, when the mass fraction values for each column were plotted against the RSD data, a linear correlation was revealed between the two (Figure 4.11). This is the same result obtained the channel variance data of the MSFs was plotted against the RSD of the MSF channel diameters. The replication of this result through CFD suggests that a direct linear relationship exists between the two properties.

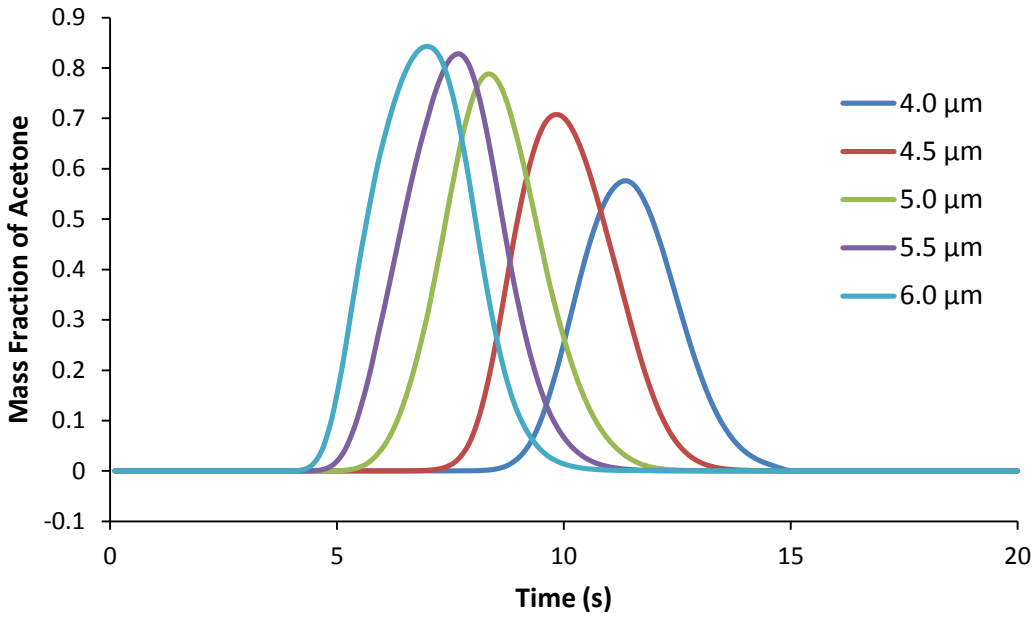

Figure 4.9: Pseudo-chromatogram of the mass fraction of acetone over time for the individual channels in column E. The channel diameters corresponding to each peak are given in the legend.

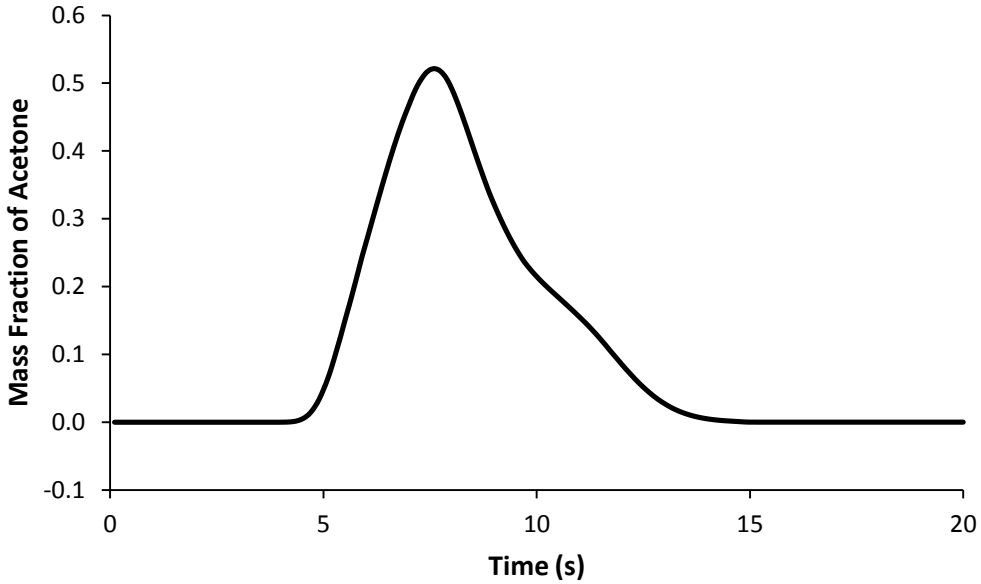

Figure 4.10: Pseudo-chromatogram of the sum of the area-weighted averages for the mass fraction of acetone over time through each channel for column E.

Table 4.3: Peak width data acquired for five-channel columns A-E.

Column	*A*	*B*	*C*	*D*	*E*
Peak Start (s)	5.4	5.3	5.2	5.3	4.6
Peak End (s)	10.9	11.1	11.3	12.5	13.6
Peak Width (s)	**5.5**	**5.8**	**6.1**	**7.2**	**9.0**

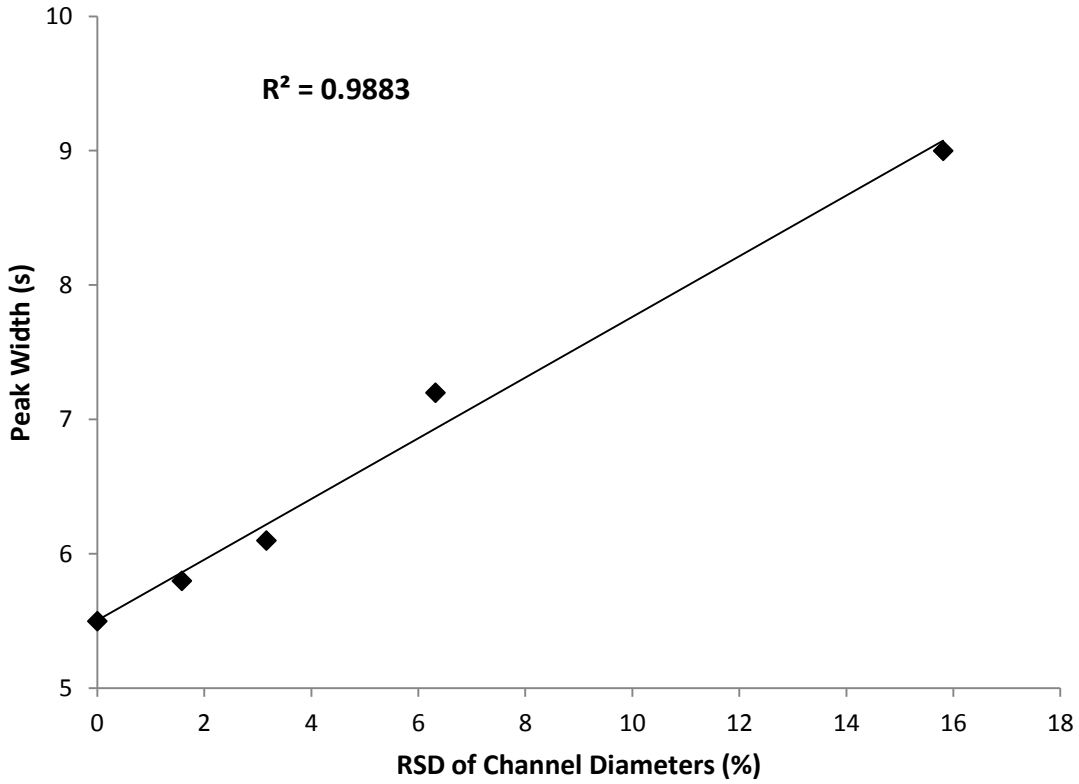

Figure 4.11: Correlation plot between the mass fraction values of acetone for each column against the RSD of the channel diameters.

4.4 Conclusions

Through the use of CFD, a computer protocol capable of simulating flow velocity distributions in multi-channel columns was successfully designed and implemented. Using the ANSYS software, simplified columns containing two or five channels of differing sizes were virtually constructed and, using a UDF, it was possible to model the passage of a pulsed injection of acetone through the columns and assess the flow velocities inherent in each channel based on its size. From these simulations, pseudo-chromatograms tracking the mass fraction of acetone at the channel outlets were generated, which exhibited results that, as expected, featured higher flow velocities in the larger channels. Furthermore, the results were very similar to the data obtained in previous research associated with the characterization of MSFs via HPLC, following similar trends in both the effect of longer channel lengths as well as differences in RSD of the channel diameters.

Suggestions for future work largely entail further refinement of the simulation setting to more realistically model microfluidic flow. The primary issue that should be addressed is how to properly incorporate diffusion into the simulations. The current setup, which resorts to artificially low diffusion coefficients that remove diffusion altogether, is erroneous and was used simply to circumvent the extreme diffusion that was otherwise encountered. To obtain more rigorous and realistic data, the diffusion coefficient should be properly set and the mixing laws properly defined. This would require a better understanding of the mixing laws used by the software in order to

properly correct this. Furthermore, the simulation currently does not account for chemical interactions between the fluid and the channel walls. Since this is a major factor in the parabolic flow profiles observed in real microfluidic flow, it should also be implemented into the protocol. Finally, geometries with increasingly longer and more channels should be designed and tested in order to better model MSFs. The primary challenge in accomplishing this is addressing the error encountered when the column volume is too large to implement the appropriate mesh.

Chapter 5: Conclusions and Future Work

The goal of this project was to address the two primary sources of flow velocity variation in MSFs when applied as supports for OTLC; namely, introduction of the stationary phase and differences in channel size. Regarding stationary phase introduction, past research in the Oleschuk group clearly illustrated the difficulties associated with preparing films for OTLC in an equal fashion among the channels. Thus, in an effort to circumvent the issue altogether, the bare silica walls of the MSF channels were promoted to the role of stationary phase for separations in HILIC mode. Unfortunately, the channel walls were insufficient in sustaining a significant retentive mechanism. Based on the result, it is clear that the channel walls must be functionalized in order to supply retention. Future work should return to the development of monolayers as stationary phase films for OTLC, given their superior performance over other techniques that have been attempted.

With respect to size distribution among the MSF channels, its influence on flow velocity inhomogeneity depends chiefly upon how the MSFs are manufactured. Since the manufacturing procedure is not a controllable variable, efforts were instead focused on further investigating the relationship between channel variance and flow variation. An experimental procedure was designed to quantify this relationship through a chromatographic approach using UPLC in the absence of a retentive mechanism, which afforded very wide peaks. It was found that the resulting peak widths were dependent upon the degree of channel variance inherent in the MSF used. Furthermore, a

correlation was revealed between the RSD of the channel diameter and the corresponding peak widths, suggesting that a linear relationship exists. This was reinforced through the use of CFD – replication of the experiment computationally also afforded a linear correlation between peak width and channel diameter.

To summarize, the experiments outlined in this study serve to provided further insight into the nature of fluid flow in multi-channel supports, and specifically, how differences in flow velocity negatively impacts the column efficiency when applied to chromatography. With continued refinement of the procedures, it should be possible to attain more accurate and precise measurements which will further elucidate the relationship between flow inhomogeneity and chromatographic performance. The data from these experiments would benefit future work in the use of MSFs as multi-channel supports for OTLC.

References

1. Ettre, L. S. *Pure & Appl. Chem*. **1993**, *65* (4), 819.

2. Harris, D. C. *Quantitative Chemical Analysis, 7e*; W. H. Freeman and Co.: New York, 2006.

3. Skoog. D. A.; Holler, F. J.; Crouch, S. R. *Principles of Instrumental Analysis, 6e.* Thomson Brooks/Cole: Belmont, CA, 2007.

4. Martin, A. J. P.; Synge, R. L. M. *Biochem J.* **1941**, *39*, 1358.

5. Kennedy, G. H.; Knox, J. H. *J. Chromatogr. Sci.* **1972**, *10*, 549.

6. Horvath, C.; Lin, H. J. *J. Chromatogr. Sci*. **1976**, *126*, 401.

7. Giddings, J. C. *Dynamics of Chromatography, Part I: Principles and Theory, Chromatographic Science Theory*; Marcel Dekker, Inc.: New York, 1965.

8. van Deemter, J. J.; Zuiderweg, F. J.; Klinkenberg, *Chem. Eng. Sci.* **1965**, *5*, 271.

9. Brown, P. R. *Anal. Chem.* **1990**, *62* (19), 995A.

10. Quintin, T. J. *Chromatography* **2010**, 103.

11. Bester, K. *Anal. Bioanal. Chem.* **2008**, *391* (1), 15.

12. Jena, A. K. *Pharm. Anal. Acta* **2012**, *3* (1), 147.

13. Tang, X.; Xaio, X. *Dangdai Huagong* **2011**, *40* (9), 988.

14. Toomula, N.; Kumar, A.; Kumar, D.; Sathish, B.; Vijaya, S. *J. Anal. Bioanal. Techniques* **2011**, *2* (5), 127.

15. Chhabil, D. *Current Organic Chemistry* **1999**, *3* (2), 193.

16. Miller, C.; Rivier, J. *Biopolymers* **1996**, *40* (3), 265.

17. Rissler, K. *J. Chromatogr. A* **1996**, *742* (1+2), 1.

18. Saczk, A. A.; Okumura, L. L.; De Oliveira, M. F.; Zanoni, M. V. B.; Stradiotto, N. R. *Anal. Bioanal. Chem.* **2005**, *381*, 1619.

19. Abian, J.; Oosterkamp, A. J.; Gelpi, E. *J. Mass Spectrom.* **1999**, *34*, 244.

20. Vissers, J. P. C. *J. Chromatogr. A* **1999**, *856*, 117.

21. Bruins, A. P. *J. Chromatogr. A* **1998**, *794*, 345.

22. Nawrocki, J. *J. Chromatogr. A* **1997**, *779*, 29.

23. Snyder, L. R.; Kirkland, J. J. *Introduction to Liquid Chromatography, 2e;* John Wiley & Sons: New York, 1979.

24. Patel, K. D.; Jerkovich, A. D.; Link, J. C.; Jorgenson, J, W. *Anal. Chem.* **2004**, *76*, 5777.

25. Jorgenson, J. W. *Annual Review of Analytical Chemistry* **2010**, *3*, 129.

26. Mellors, J. S.; Jorgenson, J. W. *Anal. Chem.* **2004**, *76*, 5441.

27. Svec, F.; Frechet, J. M. J. *Anal. Chem.* **1992**, *64* (7), 820.

28. Svec, F.; Frechet, J. M. J. *Chem. Mater.* **1995**, *7*, 707.

29. Guiochon, G. *J. Chromatogr. A* **2007**, *1168*, 101.

30. Svec, F. *J. Chromatogr. A* **2010**, *1217*, 902.

31. Alpert, A. J. *J. Chromatogr.* **1990**, *499*, 177.

32. Nováková, L.; Kaufmannová, I.; Jánská, R. *J. Sep, Sci.* **2010**, *33*, 765.

33. Jandera, P. *Anal. Chim. Acta* **2011**, *692*, 1.

34. Yoshida, T. *J. Biochem. Biophys. Methods* **2004**, *60*, 265.

35. Guo, Y.; Gaiki, S. *J. Chromatogr. A* **2011**, *1218*, 5920.

36. Ishii, D.; Takeuchi, T. *TrAC* **1990**, *9* (5), 152.

37. Novotny, M. *Anal. Chem.* **1981**, *53* (12), 1294A.

38. Halász, I.; Endele, R.; Asshauer, J. *J. Chromatogr.* **1975**, *12*, 37.

39. Ishii, D.; Asai, K.; Hibi, K.; Jonokuchi, T.; Nagaya, M. *J. Chromatogr.* **1977**, *144*, 157.

40. Yang, F.J. *J. Chromatogr.* **1982**, *236*, 265.

41. Tsuda, T.; Novotny, M.; *Anal. Chem.* **1978**, *50*, 632.

42. Reese, C.E.; Scott, R. P. W. *J. Chromatogr. Sci.* **1980**, *18*, 479.

43. MacNair, J. E.; Patel. K. D.; Jorgenson, J. W. *Anal. Chem.* **1999**, *71*, 700.

44. Fabrice, G.; Guiochon, G. *J. Chromatogr. A* **2012**, *1228*, 2.

45. Karlsson, K.-E.; Novotny, M. *Anal. Chem.* **1988**, *60*, 1662.

46. Kennedy, R. T.; Jorgenson, J. W. *Anal. Chem.* **1989**, *61*, 1128.

47. Hernández-Borges, J.; Aturki, Z.; Rocco, A.; Fanall, S. *J. Sep. Sci.* **2007**, *30*, 1589.

48. Vissers, J. P. C.; Claessens, H. A.; Cramers, C. A. *J. Chromatogr. A* **1997**, *779*, 1.

49. Wilm, M.; Mann, M. *Int. J. Mass Spectrom. Ion Processes* **1994**, *136*, 167.

50. Sanchez, A. C.; Anspach, J. A.; Farkas, T. *J. Chromatrogr. A* **2012**, *1228*, 338.

51. Gritti, F.; Sanchez, A. C.; Farkas, T.; Guiochon, G. *J. Chromatogr. A* **2010**, *1217*, 3000.

52. Chervet, J. P.; Ursem, M.; Slazmann, J. P. *Anal. Chem.* **1996**, *68*, 1507.

53. Vissers, J. P.; de Ru, A.; Ursem, M.; Chervet, J. P. *J. Chromatogr.* **1996**, *746*, 1.

54. Swart, R.; Kraak, J. C.; Poppe, H. *TrAC* **1997**, *16* (6), 332.

55. Francotte, E.; Jung, M. *Chromatographia* **1996**, *42*, 521.

56. Guiochon, G. *Anal. Chem.* **1981**, *53*, 1318.

57. Jorgenson, J. W.; Guthrie, E. J. *J. Chromatogr.* **1983**, *255*, 335.

58. Swart, R.; Kraak, J. C.; Poppe, H. *Chromatographia* **1995**, 587.

59. Causon, T. J.; Shellie, R. A.; Hilder, E. F.; Desmet, G.; Eeltink, S. *J. Chromatogr. A* **2011**, *1218*, 8388.

60. Liu, G.; Djordjevic, N. M.; Erni, F. *J. Chromatogr.* **1992**, *598*, 153.

61. Greibrokk, T.; Andersen, T. *J. Chromatogr. A* **2003**, *1000*, 743.

62. Luo, Q.; Yue, G.; Valaskovic, G. A.; Gu, Y.; Wu, S.-L.; Karger, B. L. *Anal. Chem.* **2007**, *79*, 6174.

63. Marcus, R. K. *J. Sep. Sci.* **2008**, *31*, 1923.

64. Tao, D.; Zhang, L.; Shan, Y.; Liang, Z.; Zhang, Y. *Anal. Bioanal. Chem.* **2011**, *399*, 229.

65. Rogeberg, M.; Wilson, S. R.; Greibrokk, T.; Lundanes, E. *J. Chromatogr. A* **2010**, *1217*, 2782.

66. She, Y.; Page, J. S.; Smith, R. D. *Adv. In Chromatogr.* **2009**, *47*, 31.

67. Wang, D.; Hincapie, M.; Rejtar, T.; Karger, B. L. *Anal. Chem.* **2011**, *83*, 2029.

68. Meyer, R. F.; Champlin, P. B.; Hartwick, R. A. *J. Chromatogr. Sci.* **1983**, *21*, 433.

69. Janik, A. *J. Chromatogr. Sci.* **1976**, *14*, 589.

70. Pierce, H. D.; Unrau, A. M.; Oehlschlager, A. C. *J. Chromatogr. Sci.* **1979**, *17*, 297.

71. De Nevers, N. *Fluid Mechanics for Chemical Engineers*, 3rd ed.; McGraw-Hill: New York, 2005.

72. Rudenko, B. A.; Shoromov, N. P.; Kumakhov, M. A.; Naida, O. O. *J. Anal. Chem.* **2005**, *60* (10), 956.

73. Naida, O. O.; Rudenko, B. A.; Khamizov, R. Kh.; Kumakhov, M. A. *J. Anal. Chem.* **2009**, *64* (7), 721.

74. Patrushev, Y. V.; Nikolaeva, O. A.; Sidelnikov, V. N. *J. Anal. Chem.* **2010**, *65* (11), 1129.

75. Russell, P. *Science* **2003**, *299* (5605), 358.

76. Joannopoulos, J. D.; Johnson, S. G.; Winn, J. N.; Meade, R. D. *Photonic Crystals: Molding the Flow of Light*, 2nd ed. Chapter 9. Princeton University Press, 2008.

77. Sun, Y.; Nguyen, N.-T.; Kwok, Y. C. *Anal. Bioanal. Chem.* **2009**, *394*, 1707.

78. Matajec, V.; Podrazky, O.; Hayer, M.; Pospisilova, M.; Berkova, D. *Proceedings of SPIE* **2008**, *7138*, 713806/713801.

79. Su. S.; Gibson, G. T. T.; Mugo, S. M.; Marecak, D. M.; Oleschuk, R. D. *Anal. Chem.* **2009**, *81*, 7281.

80. Daley, A. B.; Wright, R. D.; Oleschuk, R. D. *Anal. Chim. Acta* **2011**, *690*, 253.

81. Irving, R. A. *Exploring the Use of Microstructured Fibres as a Stationary Phase Support for Open Tubular Liquid Chromatography.* (2011). MSc Thesis. Queen's University, Kingston, ON. 76pp.

82. Naidong, W. *J. Chromatogr. B* **2003**, *796*, 209.

83. Marrubini, G.; Mendoza, B. E. C; Massolini, G. *J. Sep. Sci.* **2010**, *33*, 803.

84. Daley, A. B. *Development of New Fluorous Stationary Phase Technologies for Improved Analytical Separations.* 2011. PhD thesis. Queen's University, Kingston, ON. 159pp.

85. Bakry, R.; Stoeggl, W. M.; Hochleitner, E. O.; Stecher, G.; Huck, C. W.; Bonn, G. K. *J. Chromatogr. A* **2006**, *1132*, 183.

86. Courtois, J.; Szumski, M.; Bystroem, E.; Iwasiewicz, A.; Shchukarev, A.; Irgum, K. *J. Sep. Sci.* **2006**, *29*, 14.

87. Young, H. D.; Freedman, R. A. *University Physics (with Modern Physics)*, 11th ed. (2004) Pearson Education: San Francisco, CA.

88. Prüß, A.; Kempter, C.; Gysler, J.; Jira, T. *J. Chromatogr. A* **2003**, *1016*, 129.

89. Kuipers, J. A. M.; Swaaig, W. P. M. *Adv. Chem. Eng.* **1998**, *24*, 227.

90. Kamyar, A.; Sandur, R.; Hasanuzzaman, M. *International Journal of Heat and Mass Transfer* **2012**, *55* (15-16), 4104.

91. Gurau, V.; Mann, J. A. *SIAM Journal of Applied Mathematics* **2010**, *70* (2), 410.

92. Wendt, J. F. *Computational Fluid Dynamics: An Introduction (3e)*. Von Karman Institute. Springer-Verlag: Berlin, 2009.

93. Schott Lithotec AG. Material Safety Data Sheet, Fused Silica (Mar 15 2006). http://www.itos.de/dateien/fusedsilica/msds_fused_silica.pdf. Accessed June 5 2012.

94. GSI Environmental Chemical Database. Acetone Physical Properties. http://www.gsi-net.com/en/publications/gsi-chemical-database/single/4.html. Accessed June 5 2012.

Appendix A: UDF code for specification of mass fraction of acetone over time at inlet

This file, when interpreted by Fluent and hooked to the mass fraction of a boundary face, will set the mass fraction of the solute component to 0 for all flow times outside the plug insertion window and 1 for all flow times inside it.

```
#include "udf.h"

DEFINE_PROFILE(massfrac, thread, position)
{

  float t, frac;
  face_t f;

  t = RP_Get_Real("flow-time");

 if (t<053)
    frac = 0.;
  else
    if (t>2.)
    frac =  0.;
  else
     frac = 1.;
  begin_f_loop(f, thread)
  {
   F_PROFILE(f, thread, position) = frac;
  }
  end_f_loop(f, thread)

}
```